Diamond Thin Films Handbook

Chapter 4

David S. Dandy
Department of Chemical Engineering
Colorado State University
Fort Collins, Colorado 80523

Michael E. Coltrin
Chemical Processing Sciences Department
Sandia National Laboratories
Albuquerque, New Mexico 87185

To appear in
Diamond Thin Films Handbook
J. Asmussen & D. Reinhard, Editors
Marcel Dekker, Inc.

Table of Contents

I. Introduction 3
II. Gas-phase processes in CVD diamond 4
A. Gas-phase chemical kinetics 5
B. Reactions at a hot filament 6
C. Plasma activation of the gas phase 8
III. Surface chemistry in CVD diamond 10
A. Calculation of diamond surface structures and energetics 10
B. H-abstraction / radical termination reactions 12
C. Growth chemistry 14
D. Reduced reaction mechanisms 19
IV. Nucleation Phenomena 22
A. Nucleation mechanisms 23
1. Homogeneous nucleation 23
2. Heterogeneous nucleation 24
B. Diamond epitaxy and morphology evolution 29
1. Epitaxy 29
2. Oriented growth 30
3. Morphology evolution 32
C. Effects of surface conditions 33
D. Effects of deposition conditions 36
1. Substrate temperature 36
2. Reactor pressure 36
3. Reactant composition 37
V. In situ diagnostics 38
A. Hot-filament deposition 39
B. Plasma-assisted deposition 44
C. Combustion flame deposition 48
VI. Reactor scale modeling 50
A. Hot-filament reactors 51
B. Plasma-assisted reactors 58
C. Combustion reactors 61
VII. Summary 62
Acknowledgments 63
References 64

Chapter 4 Deposition Chemistry: Deposition Pathways, Nucleation, and Growth

I. Introduction

The unique properties of diamond, such as hardness and high thermal conductivity, make it an important new material in a wide range of applications, for example, protective coatings and thermal management. However, the high cost of material production has limited the commercial use of diamond thin films to a few, very specialized applications. In chemical vapor deposition (CVD) of diamond, the factors driving cost include low reagent utilization, low deposition rates, high energy consumption, large thermal management loads at the substrate, and capital equipment costs. For these reasons, there has been much research on the CVD diamond process, including both work on empirical process optimization and on understanding the fundamental steps in the process. The latter, more basic research is done in the expectation that knowledge of the underlying chemistry, physics, transport, and materials issues will enable optimization (and cost reduction) through model-based process design.

In this chapter a review is presented of the current understanding of diamond CVD growth mechanisms. Because diamond deposition depends on different chemical and transport processes occurring in the gas phase and on the surface, discussion of these mechanisms is separated into separate sections that focus on gas-phase processes, surface chemistry, and nucleation phenomena. Discussion has also been included on experimental and theoretical studies of diamond deposition to illustrate the insight gained from macroscopic measurements and predictions. Absent from this chapter is a discussion of alternative chemistries in diamond CVD. For example, the addition of oxygen in non-combustion systems to enhance growth rate and film quality and the use of fluorinated hydrocarbons to achieve deposition at lower substrate temperatures are both important areas of study, but these do not change the basic mechanisms controlling the growth of diamond by CVD.

II. Gas-phase processes in CVD diamond

All diamond CVD processes have in common a highly energetic activation stage in the gas phase. This stage typically serves two purposes, to dissociate the hydrocarbon precursor molecule into fragments which react more readily at the deposition surface, and to dissociate molecular hydrogen to create a super-equilibrium concentration of gas-phase hydrogen atoms. Four commonly used diamond CVD reactors to achieve the activation are: hot-filament reactors, microwave plasma reactors, dc arcjet reactors, and combustion-synthesis reactors.

Although these deposition systems vary greatly in many engineering aspects, they have many important features in common, which is why each is able to produce high-quality diamond films. A large amount of energy, in the form of electrical or chemical free energy, is input to achieve dissociation of molecular hydrogen and the hydrocarbon feedstock. Moderately low pressures (in the range 10 Torr – 1 atm), are used to prevent three-body recombination of H to form molecular hydrogen. High gas-phase temperatures, greater than 1700 ˚C, are produced in the activation zone, and passive or active cooling is employed to maintain a substrate temperature in the neighborhood of 925 ˚C.

However, transport processes are quite different among the four reactor types. Hot-filament and microwave plasma reactors are diffusion-dominated; typically there is no thermal, velocity or concentration boundary layer. Thus, one often finds linear gradients in temperature, velocity, or species concentration between the excitation region (hot filament or plasma ball) and the deposition surface in these reactors. Growth rates and other observables are a weak function of input flow rate (or velocity). On the other hand, arcjet and combustion CVD reactors are characterized by high velocities, for example, greater than 10^5 cm/s, and are thus convection dominated. Thin boundary layers in temperature, velocity, and concentration are formed near the growth surface.

A. Gas-phase chemical kinetics

The gas-phase chemistry occurring in CVD diamond synthesis involves reactions of small hydrocarbons and their dissociation fragments. The chemical kinetics of C/H/O species has been the subject of decades of experimental, theoretical and modeling research in the combustion community [1]. Thus, the gas-phase chemistry aspects of diamond growth are probably better understood than any other CVD system, with perhaps the exception of the CVD of Si from SiH_4.

Temperature and pressure-dependent rate constants for a great number of the elementary gas-phase reactions have been measured experimentally, and provide the direct input to CVD diamond kinetic models. However, in some cases rate constants for relevant reactions are not available. Sometimes use of a measured rate constant in a calculation, for example, gives a wrong prediction of flame speed or temperature. This may be because the measured rate constant itself is in error, or may be due to other unknown sources of error in the simulation.

The combustion research community has developed a number of reaction mechanism sets that have been tested and compared with experiment [2-8]. Usually some individual rate constants in a mechanism set have been adjusted such that the overall mechanism as a whole gives optimal predictions for certain types of flames. As such, it can be dangerous to extract individual reactions from one mechanism and incorporate them into another, without a thorough understanding of the limitations and validity of the particular numbers. Therefore, in searching for gas-phase reaction kinetics to use in a simulation of a CVD diamond experiment, it is best to consider published reaction sets “as a whole” and not mix-and-match information from different mechanism sets.

The reaction mechanism of Miller and Bowman [4] was developed to describe non-sooting, oxygen-acetylene flames. It contains about 150 reactions of 51 hydrocarbons up to C2 species, and is adequate for many diamond CVD applications in which the gas is rich in H-atoms, and thus formation of higher hydrocarbon species is not very important [9]. A near-sooting mechanism was created by Miller and Melius [6], which contains approximately 220 reactions among 49 chemical species. The mechanism includes reactions and species leading to the formation of benzene; it is commonly assumed benzene is a key precursor in the formation of polyaromatic hydro-

carbons and soot. The Miller-Melius mechanism may be appropriate for modeling a combustion-synthesis diamond CVD experiment under fuel-rich conditions; however, extremely fuel-rich conditions usually lead to diamond films of poor quality, and as such are of less practical importance. A very large reaction mechanism (853 reactions among 190 chemical species), including hydrocarbons up to C_8H_{18} was developed by Westbrook and Pitz [3, 7]. Recently, a consortium of researchers from several different institutions has joined to produce validated combustion reaction mechanisms, under the sponsorship of the Gas Research Institute. At the time of this writing, the latest version of the reaction set [8], GRI-Mech 2.11, contained 276 reactions of 49 species containing the elements C/H/O/N.

Wolden et al. [10] presented a brute-force sensitivity analysis of two different gas-phase reaction mechanisms, the 89-reaction mechanism of Frenklach and Wang [11] and the 24-reaction mechanism of Harris, Weiner, and Perry [12, 13], to develop a reduced gas-phase reaction mechanism. Wolden et al. used a zero-dimensional model to integrate the kinetics at a temperature of 2000 K and 20 Torr for 0.1 s; these particular conditions were chosen to mimic the conditions encountered by the gas mixture flowing past a hot-filament [14, 15]. Both of the starting reaction mechanisms reduced to the same set of 9 (reversible) gas-phase reactions, which did a good job matching time-evolution of the C_2H_2, CH_3, and H concentrations predicted by the longer reaction mechanisms. These reactions fall into three broad groups (1) the three-body recombination of atomic H, (2) interconversion reactions between CH_4 and CH_3 and (3) methyl-methyl recombination reactions, followed by hydrogen-stripping reactions to form acetylene.

A key role of hydrogen in the gas-phase chemistry of diamond CVD is to suppress formation of aromatic species [9]. Minimizing production of aromatics is assumed to inhibit formation and growth of graphitic phases on the deposition surface, and thus improve diamond film quality.

B. Reactions at a hot filament

Langmuir [16-18] first discovered the catalytic dissociation of hydrogen on a hot tungsten filament, and such a hot filament has proven to be an easily constructed, efficient H-atom source.

Matsumoto first proposed use of hot filaments for diamond CVD [19, 20]. The majority of basic research has been done on hot-filament reactors, because they can be assembled rather inexpensively on the lab-bench scale, yet can produce good quality diamond films.

A thorough investigation of H_2 dissociation at a hot-filament was conducted by Jansen, Chen, and Machonkin [21], who used the difference in power consumption by the filament in a vacuum and in hydrogen as a measure of the hydrogen dissociation rate. The dissociation rate was shown to depend on the geometry of the heater element. Relatively high dissociation rates, normalized per heater area, were obtained for small-diameter wires, and it was argued that this indicates a nonequilibrium dissociation process. A mathematical analysis of the H production rate was presented which depended upon parameters such as the diffusion coefficients, wire diameter, and dissociation rate constant.

Meier et al. [22] used two-photon laser-induced fluorescence (LIF) to determine H-atom concentrations relative to a hot filament. In this experiment there was no substrate, and thus no diamond growth was occurring. They measured [H] as a function of total pressure, distance from the filament, filament temperature, filament diameter, filament material, and CH_4 mole fraction. They found little effect on [H] due to addition of up to 5% CH_4. However, in other studies, tungsten filaments have been found to carburize during diamond CVD upon high exposure to hydrocarbon feedstock [23]. Such carburization degrades the catalytic activity for hydrogen dissociation, and gas-phase H-atom concentrations have been found to drop by at least an order of magnitude when the methane concentration is increased between a factor of 3 to 10 [15, 24-27]. As discussed in Section VI.A, Dandy and Coltrin found that inclusion of filament poisoning effects was necessary to model the gas-phase chemistry in a hot-filament reactor [28], because H-atom concentration controls the kinetics to such a large degree.

C. Plasma activation of the gas phase

Direct-current (dc) arcjet-assisted diamond CVD can attain very high growth rates [29-31] due to the high arcjet powers and material flow rates possible in these systems. Within the arcjet, electrical energy is converted to chemical free energy through dissociation of hydrogen. The degree of hydrogen dissociation is typically high, 20% or greater, but not known precisely. Detailed physical models of arcjet operation have not been included in diamond CVD models, although Dandy and Coltrin [32] gave a simple thermodynamic model of an arcjet that predicts hydrogen dissociation fraction for a specified input power and operational temperature, as illustrated in Fig. 1. Temperatures at the exit of the arcjet can be in the range 1000–4000 K [33-35]. The combination of high temperature and large concentration of atomic H produces high reaction rates of the reactant gases in the free stream below the arcjet.

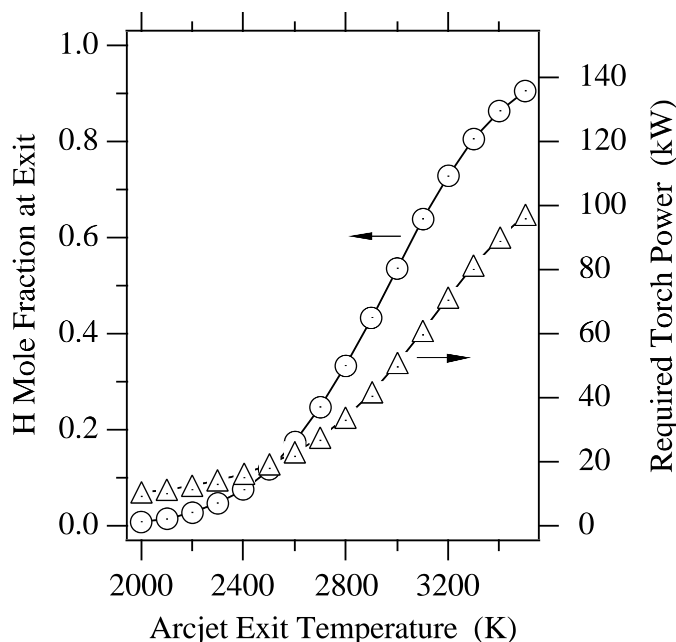

Figure 1. Predicted H-atom mole fraction exiting the arcjet and power required as a function of the arcjet operating temperature, from the thermodynamic model of Dandy and Coltrin [32].

Hydrocarbon feedstock is usually injected downstream from the exit of the arcjet. When methane is the reactant gas, the C1 species, i.e., CH_x (x = 0–4) equilibrate very rapidly [36, 37], and thus the concentration of methane is very low in the free stream. After equilibration (within a few cm of the exit of the arcjet) the C1 manifold of species remains essentially frozen in the convective free-stream until the boundary layer is encountered near the substrate. In contrast, acetylene is much more stable than methane, and when acetylene is used as the reactant gas it undergoes significantly less gas-phase decomposition. Figure 2 shows the time-evolution of species concentrations from homogeneous chemical kinetics calculations [37] under conditions typical of the free-

stream beneath the exit of an arcjet, that is, 5000 K, 3 Torr, 33% dissociated H_2. One sees significant decomposition of methane within a few μs in Fig. 2(a), while there is much less decomposition when acetylene is the reactant in Fig. 2(b).

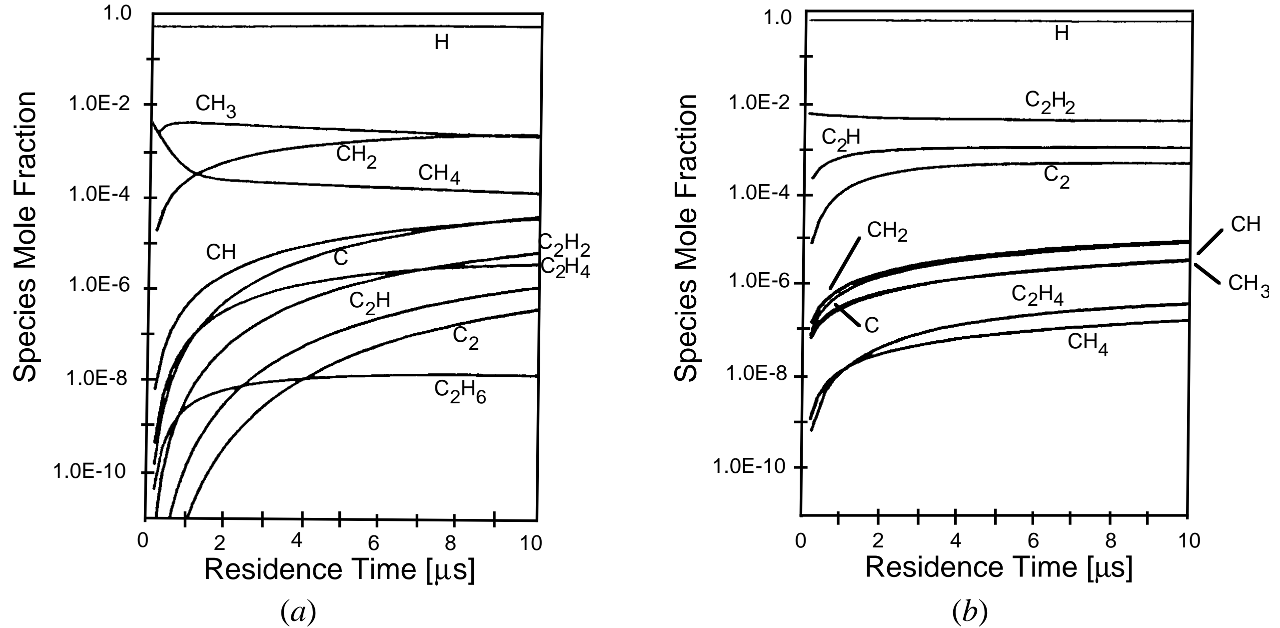

Figure 2. Kinetics simulation from Loh and Cappelli [37] of gas-phase chemistry under dc arcjet conditions for (*a*) 0.5% methane, and (*b*) 0.5% acetylene as the hydrocarbon reactant.

In a microwave plasma system, energy from the microwave electric field ionizes the gas, which is primarily H_2 with small amounts of hydrocarbon. Energy is subsequently transferred from the electrons to vibrational levels in H_2; then this vibrational energy serves to heat the gas through vibration-to-translation energy transfer to atomic H, and vibration-to-vibration or vibration-to-translation energy transfer to other H_2 molecules [38]. Ion chemistry is important in these systems as an electron-loss source. Electrons can dissociate H_2 and eventually lead to a concentration of H^+ ions, which can subsequently undergo charge-exchange with hydrocarbon and oxygen-containing species. Neutral chemistry in the gas phase is also initiated by electron-impact dissociation of H_2, O_2, and hydrocarbons [38].

III. Surface chemistry in CVD diamond

A. Calculation of diamond surface structures and energetics

Modern theoretical chemistry techniques are well-suited to study the bonding and surface structures relevant to diamond CVD, because the structures mainly consist of relatively light elements and thus few electrons, i.e., carbon and hydrogen, and because bonding is generally short-ranged and covalent, so relatively small "slabs" can be used to model the lattice. A wide array of theoretical papers have appeared which report stabilities of proposed surface structures, relative bond strengths among competing adsorbate species, reaction barriers and the like.

Mehandru and Anderson [39] used atom-superposition and electron-delocalized molecular-orbital (ASED-MO) to study adsorption energetics and bonding of CH_3, CH_2, CH, C_2H, and C_2H_2 on clean and hydrogenated {111} diamond faces. On either the clean or hydrogenated surface, the adsorption bond-dissociation energy (BDE) varied as $C_2H > CH \cong CH_2 > CH_3$. The 1:1 (complete monolayer) coverage of CH_3 was concluded to be very unstable due to steric repulsions (–2.3 eV BDE); the 1:1 coverage of CH_2, CH, and C_2H were all predicted to be stable. The favored bonding site for C_2H_2 on a clean {111} surface was di-σ bridging. Bonding to the surface via a single σ-bond was found to be very weak (1.2 eV) compared to the di-σ bond (3.5 eV).

Mehandru et al. [40] also used this technique to study hydrogen diffusion within the bulk diamond lattice. They found that a bond-centered (BC) site, that is, a C–H–C structure, was more stable than other interstitial sites (but still about 1.7 eV less stable than a gas-phase H atom plus the cluster). A minimum barrier to H-migration (1.9 eV) was found for moving from one BC site to a neighboring one, moving in the {110} plane. They also examined the stability of from 1 to 4 H atoms bound to a lattice vacancy. Up to four H's could be bound in the vacancy, with the calculated BDE energies decreasing monotonically (5.3, 4.4, 3.6, 2.5 eV) as the number of H's increases.

Alfonso et al. [41] used a combined density-functional/molecular dynamics simulation to calculate adsorption energies and minimum energy configurations for various hydrocarbons on flat {100}, flat {111}, and stepped {100} surfaces. For onefold adsorption sites, the bonding energies

ordered as follows: $C_2H > CH_2 > CH_3 > C_2H_2$; stable twofold adsorption sites were found for C_2H_2 on terrace sites and near steps on the {100} surface. Bonding to {111} surfaces was weaker than to the other two surfaces studied.

Alfonso, Ulloa, and Brenner [42] studied the adsorption of various hydrocarbons on a diamond {100}-(2×1) surface. They used molecular dynamics and a dynamical quenching technique [43] to calculate stable adsorption binding configurations based on the many-body potential energy function of Brenner [44]. Bonding was studied on a number of different types of sites: at the end of a dimer (having removed an H from the dimer); bridging across the two carbons in a broken-dimer (bridge sites); and bridging between the two ends of adjacent dimer pairs (troughs). For the flat {100}-(2×1) surface they calculated BDE's CH_2 (4.67 eV) > C_2H (4.34) > CH_3(4.18). Acetylene was bound considerably tighter at troughs (6.54 eV) than at bridge sites (3.62 eV), but the authors conclude that trough sites are much less abundant than bridge sites under steady-state conditions. The stability of hydrocarbon fragments near step edges was concluded to be very near the values calculated on flat terraces, due to the strong covalent (and short-ranged) nature of the bonding.

Angus and coworkers [45] studied nucleation of the diamond {111} plane upon the {0001} plane of graphite using energy minimization of a semi-classical Tersoff potential [46, 47]. They found very favorable energetics for an interface matching three diamond {111} planes for every two graphite {0001} planes. A mechanism was proposed which starts with graphitic or aromatic structures, which are then hydrogenated to provide nucleation sites for diamond growth.

Molecular mechanics MM2 [48] and MM3 [49] calculations were used by Harris and Goodwin [50] to calculate the free-energy change in each step of their detailed reaction mechanism on the reconstructed {100}-(2×1):H surface, which in turn was used to calculate the reaction equilibrium constant and reverse rate constant. Yang and D'Evelyn [51] used MM3 to examine the relative stabilities of the {100}-(2×1) reconstructed surface with varying degrees of hydrogenation. The monohydride phase was found to be the most stable, and was concluded to be the dominant

surface phase under CVD conditions. MM3 was also used to examine the energetics of each step in a proposed growth mechanism on the {100}-(2×1) surface [52].

Huang and Frenklach [53] used MNDO [54] to calculate reaction energetics on the {100}-(2×1) reconstruction. They found a barrier of 37 kcal for H_2-elimination from a surface dihydride to form the monohydride, and that the dihydride is approximately 80 kcal/mol higher in energy than the monohydride plus H_2(g). An alternate mechanism involving H-atom abstraction from the dihydride forming a dihydride surface radical, then H-elimination and C–C bond formation had a barrier of 49 kcal/mol, i.e., 12 kcal/mol higher than the other channel. They calculated a barrier of 80 kcal/mol for addition of CH_3 to a surface dihydride radical; carbon atoms were found to add to a monohydride radical site with less than a 20 kcal barrier, and acetylene addition to a radical site proceeded with a barrier of 41 kcal/mol.

Brenner [44] developed a potential energy surface for diamond and studied adsorption of hydrocarbon fragments on the {111} surface. The potential uses many-body terms based on Tersoff bond-order expressions [55]. Alfonso and Ulloa [56] performed molecular dynamics calculations employing the Brenner [44] intermolecular potential to study the adsorption of methyl radicals on the diamond {100} surface. The adsorption probability was found to increase with CH_3 incident kinetic energy and for normal incidence. Methyl radical did not react with a fully-hydrogenated surface. Thus, a surface radical site was required for CH_3 chemisorption. The same intermolecular potential was used by Garrison et al. [57], who discovered a low-energy reaction pathway for dimer-bond breaking and addition of CH_x ($x < 3$) on the {100}-(2×1):H surface from analysis of their molecular dynamics simulations.

B. H-abstraction / radical termination reactions

Reactions of atomic hydrogen are a dominant factor in the surface chemistry of diamond CVD. They control not only the gas-phase chemistry, and thus the nature of the reactive species reaching the growth surface, but also determine the availability of reactive sites upon the surface. In

addition, the recombination of hydrogen on the surface is an important source of heat in the system, and must be accounted for in substrate thermal management.

During deposition the diamond surface is usually hydrogen terminated. Growth is initiated by abstraction of an H from the surface, creating a reactive radical site

$$\mathrm{H}(g) + \mathrm{CH}(s) \Leftrightarrow \mathrm{H}_2(g) + \mathrm{C}^*(s). \quad (1)$$

This reaction is accompanied by the radical-termination reaction

$$\mathrm{H}(g) + \mathrm{C}^*(s) \Leftrightarrow \mathrm{CH}(s). \quad (2)$$

The net of these two reactions is heterogeneous recombination of atomic hydrogen to form H_2. Although reactions (1) and (2) are written as reversible, for all practical purposes the reverse reactions rates are negligible.

The abstraction reaction (1) is fast, but does not occur with unit probability. The rate constants for gas-surface reactions in diamond CVD mechanisms are usually estimated by analogy with gas-phase reactions. This, in essence, assumes that the diamond surface behaves like a giant hydrocarbon [58]. The gas-phase rate constant for abstraction of a tertiary hydrogen from an alkane is (in $\mathrm{cm}^3\ \mathrm{mol}^{-1}\ \mathrm{s}^{-1}$)

$$k_1 = 1.3\times 10^{14}\exp(-3674/T), \quad (3)$$

with the activation energy in K. The rate constant can be converted to a reaction probability γ using

$$k = \frac{\gamma}{\Gamma}\sqrt{\frac{RT}{2\pi W}}, \quad (4)$$

where Γ is the surface site density (taken here to be $3\times 10^{-9}\,\mathrm{mol\ cm}^{-3}$) and W is the atomic weight of H; for reactions of H-atoms,

$$\gamma = 8.25\times 10^{-13}\frac{k}{\sqrt{T}}. \quad (5)$$

Thus, the rate constant in Eq. (3) corresponds to a reaction probability of 0.14 at a typical growth temperature of 1200 K. Kinetic modeling studies of diamond CVD have used values of γ_1 span-

ning the range 0.22 [59] down to 0.0037 [11]. Molecular dynamics calculations of Brenner et al. [60] calculate an abstraction reaction probability of 0.04 at 1200 K.

A reasonable analogue of reaction (2) would be the gas-phase reaction of H with the iso-propyl radical, with a rate constant in the high-pressure limit of 2×10^{13} cm^3 mol^{-1} s^{-1} [2]. This rate constant corresponds to a probability of 0.48 at 1200 K. Previous models have used values of γ_2 ranging from essentially unity [59] to 0.016 [11]. Brenner et al. calculated a value of 0.43 for γ_2 at 1200 K [60]. Although there is quite a range in the probabilities that modeling studies have employed for reactions (1) and (2), there has been a good consensus among such models that the ratio γ_2/γ_1 should be in the range of 3 to 4 [11, 59, 61]. This ratio was predicted to be approximately 11 via molecular dynamics molecular [60].

A steady-state analysis [62] shows that the probabilities for reactions (1) and (2) can be combined to yield an effective probability, γ_{H}, for H-H recombination,

$$\frac{1}{\gamma_{\mathrm{H}}} = \frac{1}{2}\left(\frac{1}{\gamma_1} + \frac{1}{\gamma_2}\right). \tag{6}$$

Using the probabilities deduced from the gas-phase analogs above in Eq. (6) yields an effective recombination probability $\gamma_{\mathrm{H}} = 0.22$. Krasnoperov et al. [63] measured an effective H-atom recombination probability of 0.16; Harris and Weiner [64] measured a slightly smaller value, γ_{H}= 0.12, with about a factor of two uncertainty. Thus, we conclude that the rate constants (or equivalently) probabilities for H-atom abstraction and termination reactions derived from their gas-phase analogues are reasonable, but perhaps are as much as a factor of 2 too large.

C. Growth chemistry

The surface chemical reaction mechanism leading to diamond growth has been the subject of much research, debate, and controversy. It was widely assumed that the "correct" reaction mechanism could be found, because diamond is a relatively simple material system: it is dominated by short-range covalent bonds, chemically related to well-known hydrocarbon chemistry, and is ame-

nable to theoretical or first-principles calculation of energetics and reaction rates. However, a universally accepted diamond-growth reaction mechanism has still not yet been found. As an example, much controversy has reigned about the identification of the dominant precursor species leading to growth. In a hot-filament reactor environment, the most abundant gas-phase hydrocarbon species are C_2H_2 and CH_3, and attention focused on these two candidates as the dominant growth species. Many conflicting experiments have concluded that one species or another could or could not account for diamond growth.

It is unlikely that there is a single, simple diamond growth mechanism that applies to all deposition conditions. For example, the gas-phase environment present in a dc arcjet reactor is very different than in a hot-filament reactor; there is no *a priori* reason to expect that the same growth mechanism will be operative under such different conditions.

The first proposal of C_2H_2 as a growth species was by Frenklach and Spear [58]. A detailed kinetic reaction mechanism for diamond growth was proposed by Frenklach and Wang [11]. Their model was applied primarily to a hot-filament environment, and included acetylene as the dominant growth species. However, short-comings of the acetylene-addition mechanisms were discovered [65]. Addition of acetylene to a monoradical surface site is thermodynamically unstable: the adduct formed has too short a lifetime to allow incorporation into the diamond lattice. Addition of acetylene to a biradical site on the {111} or {110} surface forms a thermodynamically stable molecule. However, the admolecule quickly desorbs after reaction with a gas-phase H-atom, followed by a β-scission cleavage of its surface C–C bond [66]. Alternate reaction schemes for acetylene on the dimerized {110} surface have been proposed which do not suffer from the above deficiencies [65, 66].

Cappelli and Loh conducted experiments in an arcjet reactor with C_2H_2 feed gas, and reported high-quality diamond growth [67]. Under these conditions, the concentration of C1 species was too low to account for observed growth. They concluded that C_2H_2 was the dominant growth species in this experiment. In a different growth environment, the opposite conclusion was drawn. Chu et al. [68, 69] used a mixture of ^{13}C-labeled methane and ^{12}C acetylene for growth rate ex-

periments in a hot filament reactor. They measured homoepitaxial growth rates on different crystal faces of 0.4 μm/h on the {100} face, 0.5 μm/h on the {111} face, and 1.3 μm/h on the {110} face. The ^{13}C fraction in the deposited film matched that of the gas-phase methyl radical (as deduced from mass spectrometry probe sampling), and differed significantly from the ^{13}C fraction in the acetylene. From this observation they conclude that CH_3 was the dominant growth species in the hot-filament experiment. A number of other experimental papers also concluded that C_2H_2 is not a viable growth species [69-73].

There has not been a well-accepted mechanism proposed for growth on {111} planes [74, 75]. Steric repulsion appears to rule-out complete coverage of the {111} plane by methyl radicals [39]. There is only moderate repulsion between just a pair of adjacent surface CH_3 groups on the {111} plane [39, 76, 77], and such a configuration has been examined as a growth route. Atomic hydrogen abstraction from a single one of the adjacent methyls, followed by bridging reactions is limited by a high activation barrier, approximately 50 kcal/mol [77]. Abstraction of an H from both adjacent methyls would be followed by rapid formation a C–C bond, and thus a surface species such as $–CH_2–CH_2–$. However, subsequent abstraction of an H from this species will be followed quickly by β-hydride elimination of H and desorption of the $–CH{=}CH_2$ group [74]. Such a series of reactions has made drafting of a complete growth mechanism on the {111} and {110} planes difficult to date.

Frenklach et al. have proposed an atomistic model for step-flow growth upon a {100} facet between two {111} planes. The model is based on bridging methylene, CH_2, as the mobile species. However, instead of migrating via surface diffusion, CH_2 moves through a sequence of covalent bond breaking and formation [74].

Butler and Woodin [78] propose a detailed reaction sequence for growth of diamond from CH_3 (used as a “generic” growth species) on the {110} crystal face. In particular their mechanism focuses upon reactions among chemisorbed species. Kinetic rate constants for the individual steps in the mechanism were not given, and thus it has not been further incorporated into numerical kinetic or reactor-scale models.

Harris proposed a widely used mechanism for growth on the unreconstructed {100} plane with CH_3 as the growth species [59]. Rate constants for the 12 reactions in the mechanism were mainly deduced from gas-phase analogs. Thermochemistry for each reaction, i.e., ΔG, and thus the equilibrium constants and reverse rate constants, was estimated using the bicyclo[3.3.1] nonane molecule as a model of the diamond surface. Steps in this mechanism are illustrated in Fig. 3. Methyl radical (denoted by "M" in the figure) was assumed to adsorb on a surface radical site, followed by H-abstraction from both the adsorbed methyl ("M*") and an adjacent surface H, and rapid formation of a C–C bond ("bi-radical pairing"). The Harris mechanism was used quite widely to simulate CVD diamond growth in a broad range of growth conditions, including hot-filaments, oxygen-acetylene flame, dc arcjet, and rf torch reactors; see Ref. [50] for a summary.

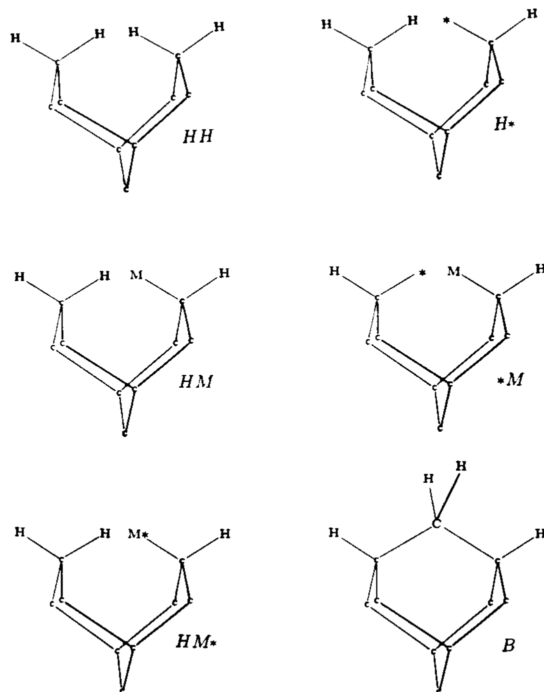

Figure 3. Steps in the methyl-addition growth mechanism of Harris [59], which uses the bicyclo [3.3.1] nonane molecule as a model of the unreconstructed {100} surface.

Steric crowding makes it very unlikely that the methyl radical can actually bond to the unreconstructed {100} surface [53], and so the original mechanism as proposed by Harris is probably not correct in all of its detail. In fact, it is unlikely that the unreconstructed {100} surface exists at all under growth conditions, due to steric repulsion between adjacent H atoms. The {100}-(2×1) reconstruction has been observed experimentally [79-82], and the stability of this surface has been examined theoretically [51].

Harris and Goodwin [50] proposed a growth mechanism on the {100}-(2×1):H (hydrogen-covered reconstruction) surface, illustrated in Fig. 4. The mechanism consists of two main parts: insertion into dimer bonds according to the route proposed by Garrison et al. [57], shown in Figs. 4(b) and (c); and bridging across the trough between the ends of two dimers, as in Fig. 4(f). The

latter part of this mechanism basically follows the steps in Harris' original methyl-addition mechanism [59]. Harris and Goodwin give rate constants for each step in their mechanism, and the corresponding thermochemistry, calculated via the molecular mechanics code MM3 [49]. Kinetic simulations showed that the trough portion of the mechanism was rate-limiting, because that portion required more H-abstraction steps than the dimer-addition portion. This mechanism was used by Harris and Weiner [83] in simulating the pressure- and temperature-dependence of diamond growth.

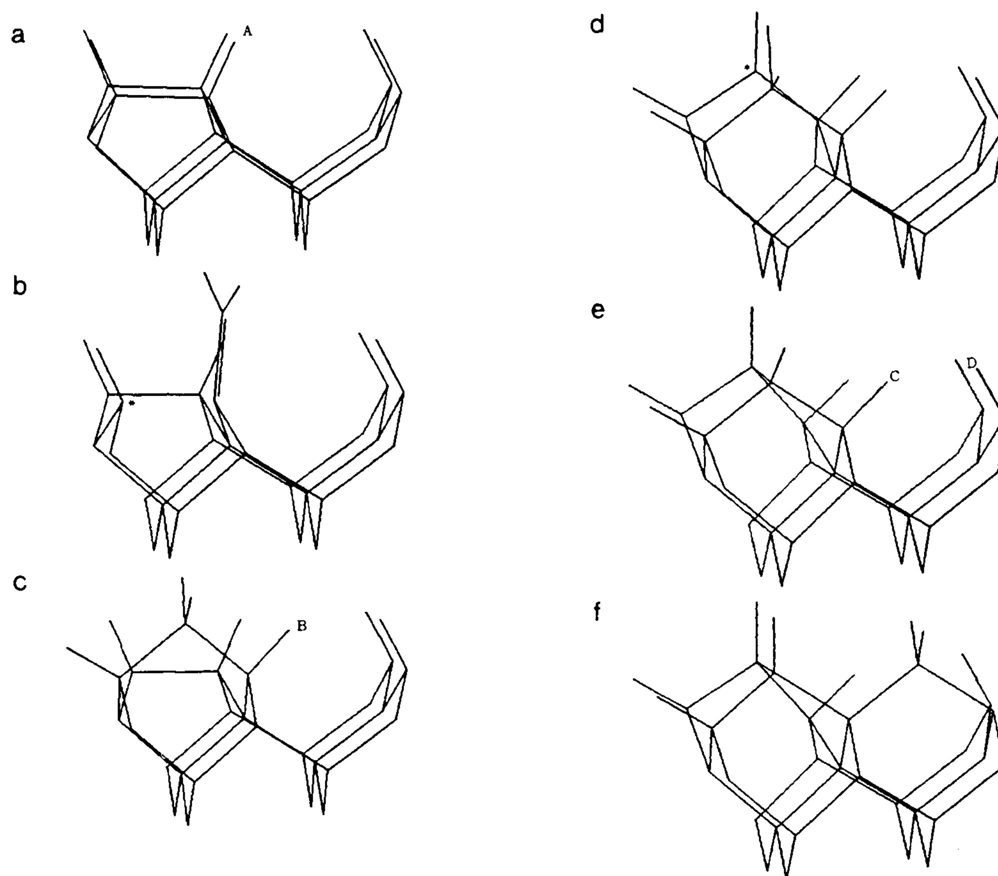

Figure 4. Steps in the mechanism proposed by Harris and Goodwin [50] for growth on the {100}-(2×1):H surface. In parts (*a*), (*c*) and (*e*), the letters "A–D" represents either an H or a surface radical site at which reaction can take place.

There is experimental evidence that surface diffusion is operative on the diamond surface at high temperatures [84-87]. Theoretical analysis of surface diffusion of H atoms, hydrocarbon species, and radical sites found these processes to be very facile [88]. Surface diffusion will be enhanced at higher temperatures, potentially leading to smoother films. However, higher tempera-

tures also lead to increased desorption from the surface and etching. The surface diffusion mechanism was also found to be unstable; the system was found to switch suddenly from a regime of smooth growth to formation of pits.

D. Reduced reaction mechanisms

The fine details of diamond growth mechanisms are very complex, still under debate, and dependent upon crystallographic plane and growth condition. However, many general aspects of diamond growth surface chemistry appear to be generic to the process and are widely agreed upon. As a result a number of simplified models of diamond growth have been developed [32, 62, 67, 78, 89]. Although not intended to be mechanistically rigorous in detail, these models attempt to explain some of the overall behavior of the diamond CVD system, e.g., scaling of growth rate, surface coverage, defect formation, energy consumption, in terms of generic reactions taking place. Such models are typified by the discussion given by Butler and Woodin [78], whose simple analysis included reactions for H-atom abstraction and radical termination, incorporation of chemisorbed hydrocarbon species into the lattice, diamond growth, and parasitic growth of defects. This model is perhaps distinguished from some of the others in discussing the surface-temperature dependence of these processes. One of the quantities predicted by the model is quality, which was defined to be the ratio of the rate at which adsorbed carbons completed their lattice bonds before being overgrown to the total rate of carbon adsorption. Figure 5 illustrates the dependence of quality on substrate temperature for two different reactor types. Case (*a*) is representative of a dc arcjet system, for which the

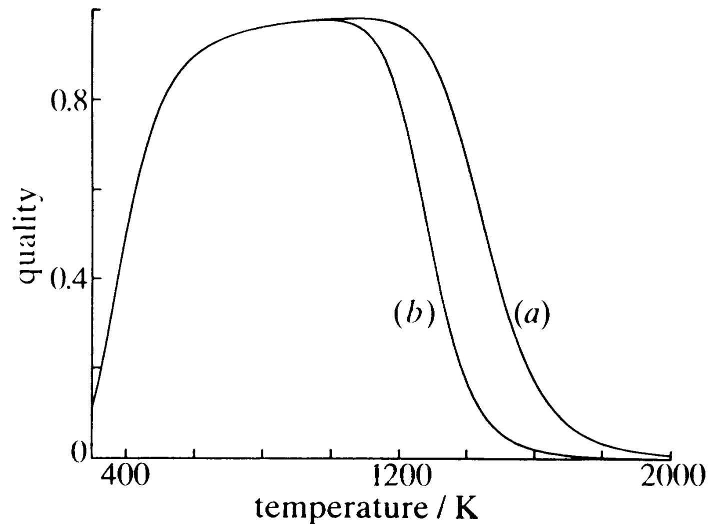

Figure 5. Calculated quality (lattice incorporation/carbon addition) as a function of substrate temperature for conditions characteristic of (*a*) dc arcjet and (*b*) hot-filament, from the model of Butler and Woodin [78].

atomic hydrogen mole fraction at the surface was assumed to be 0.1, and the mole fractions of hydrocarbons were assumed to total 10^{-4}. Case (*b*) represents conditions in a hot-filament reactor, with a near-substrate H mole fraction of 0.01 and C_xH_y mole fractions of 10^{-5}.

Goodwin [62] presented a simplified surface reaction mechanism which includes many of the important features present in more detailed kinetic schemes, including H-atom abstraction and termination reactions, addition of CH_3 to a surface radical site and a bi-radical pairing reaction to form a surface C–C bond. The mechanism also included an alternate reaction path for formation of a buried defect, for example hydrogen or sp^2 species trapped in the lattice. The simplified reaction scheme can be solved analytically, yielding expression for deposition rate and lattice-defect fraction as a function of CH_3 and H concentrations at the surface. The deposition rate expression containing two adjusted constants reproduces measured diamond growth rates from a wide range of experiments spanning growth rates from 0.1 to more than 7000 μm/h is

$$G = 1.8 \times 10^{11} \frac{[\mathrm{CH_3}][\mathrm{H}]}{5 \times 10^{-9} + [\mathrm{H}]}, \tag{7}$$

where G is the growth rate in μm/h, and the concentrations are in mol/cm^3. Assumptions in the analysis lead to the conclusion that the mole fraction of defects in the grown film, X_{def}, will scale as

$$X_{\mathrm{def}} \propto \frac{G}{[\mathrm{H}]^2}. \tag{8}$$

The form of Eq. (8) is especially important in trying to optimize diamond growth conditions. It illustrates the fundamental trade-off between achievable growth rate and film quality, i.e., defect density increases linearly with growth rate. Equation (8) predicts that growth rates can be increased quadratically with H-atom concentration for a fixed defect density. (This is achieved by simultaneously increasing the hydrocarbon fraction.) Goodwin points out that the scaling of defect fraction with H-atom concentration is uncertain, and depends upon the form of the (unknown) defect-formation reaction. He gives a more general scaling relationship for defect fraction as

$$X_{\mathrm{def}} \propto \frac{G}{[\mathrm{H}]^n}. \tag{9}$$

Dandy and Coltrin [32] discussed diamond growth in terms of a simplified growth mechanism that extended the one given by Goodwin [62] to account for growth from atomic C-atoms, which were quite abundant in the dc arcjet environment being modeled [36]. They also included a kinetic pathway for formation of lattice point-defects due to over-growth of surface hydrogen species, and thus incorporation of hydrogen into the lattice as a defect. As shown in Fig. 6, the scaling of defect fraction was found to follow (very nearly) a linearly scaling with [H], that is,

$$X_{\mathrm{def}} \propto \frac{G}{[\mathrm{H}]}, \tag{10}$$

when the defect-formation reaction was first-order with respect to surface species as reactants. When the reaction responsible for defect-formation was assumed to be bimolecular with respect to surface species, a quadratic scaling as in Eq. (8) was obtained, which is also illustrated in Fig. 6. The difference in scaling-laws for defect-formation has important implication for scaling a CVD diamond reactor to higher arcjet power, for example. If defect formation decreases approximately linearly with [H], as in Eq. (10), higher power and thus increased H-atom production would allow a linear increase in attainable growth rate (holding diamond quality fixed). However, if defect-formation scales as in Eq. (8), any increase in [H] is rewarded with a quadratic increase in the attainable growth rate (again, for fixed quality).

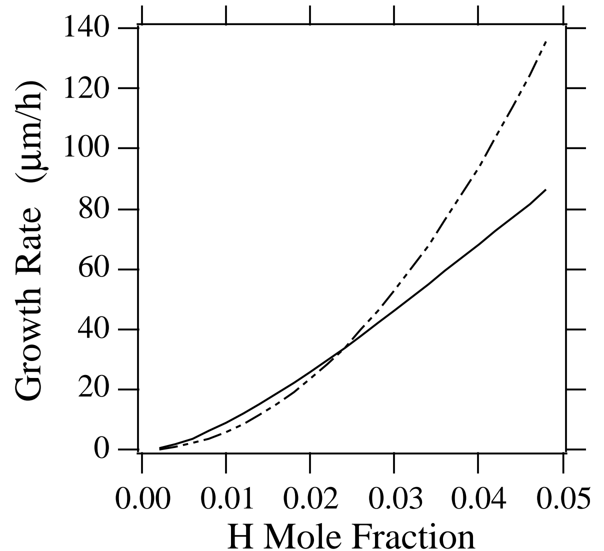

Figure 6. Predicted growth rate as a function of gas-phase H mole fraction at the surface for a fixed diamond quality (defect concentration). Solid curve is for a defect-formation reaction that is first-order in surface reactant species; dashed curve is for a defect-formation reaction that is bimolecular in surface species [32].

Angus and Edwards [89] present a simple reduced reaction set to describe many aspects of CVD diamond growth. Their model includes growth of diamond from graphitic nucleation sites [45], conversion of sp^2 sites to sp^3 hybridization and gassification of hydrogenated surface species by atomic hydrogen. The reaction scheme can be solved analytically at steady state to predict growth rates of both diamond and sp^2 impurities as a function of the concentration of a growth precursor, [CH_x], and atomic hydrogen, [H]. The model predicts that the impurity concentration will increase with [CH_x] and thus with increasing growth rate, and it will decrease more than linearly with [H].

IV. Nucleation phenomena

It has become clear in research of diamond film growth that control of the fundamental phenomena associated with diamond nucleation and the early stages of growth is essential for applications in which material properties are sensitive to, or depend directly upon, the morphology of the polycrystalline film. Film anisotropy, grain size, and nano-, micro-, and macroscopic voids all strongly affect material properties such as thermal conductivity and optical transmissivity. Indeed, if diamond is ever to be used in semiconductor applications, it will be necessary to synthesize large-area, thick, single-crystal films. An increase in surface nucleation density may reduce morphological instabilities and surface roughness, and further, may improve the homogeneity of films and reduce formation of voids at the substrate or coating interface, leading to better diamond-substrate adhesion.

Most early studies of the low pressure CVD of polycrystalline diamond have focused on studying different deposition techniques and correlating these techniques with the material properties of the resulting films. These efforts have been successful in gaining a qualitative and semi-quantitative understanding of how diamond is deposited from the gas phase. Another result of such studies has been an increasing awareness of the extreme variability in film morphology and crystallinity that could be produced with seemingly minor changes in the growth environment. Because of this observation, increasing attention has been paid to the nucleation and early growth

stages of diamond; these nucleation studies have significantly contributed to understanding of diamond nucleation mechanisms in CVD. In this section possible mechanisms for diamond nucleation will be discussed, and the effect of surface conditions and the growth environment on epitaxy, morphology evolution, and texture will be considered.

A. Nucleation mechanisms

1. Homogeneous nucleation

The emphasis of most studies on nucleation and growth of diamond has been the heterogeneous formation of diamond particles, and the crystallization and deposition of diamond films on substrate surfaces. Only limited work has been done to examine the possibility of achieving homogeneous nucleation in the gas phase at subatmospheric pressures. However, there is evidence that, at least in some cases, diamond may be nucleated homogeneously in the gas phase [90-93]. The primary reason that homogeneous nucleation of diamond has not been pursued more aggressively is that using a CVD process to produce diamond powder via homogeneous nucleation does not appear commercially competitive with other techniques, because of the low nucleation rate; and conditions conducive to homogeneous nucleation are not favorable for film growth, so it may not even be practical to use the homogeneous nucleation phenomenon as a seeding technique.

Classical nucleation theory indicates that homogeneous nucleation of diamond is possible [94], and a number of suggestions have been made regarding possible hydrocarbon cage molecules (such as adamantane) that may serve as gas phase precursors for the diamond nuclei [95]. The adamantane molecule represents the smallest combination of carbon atoms which possesses the diamond unit structure, that is, three six-membered rings in a chair structure. However, chemical equilibrium calculations reveal that proposed precursors such as adamantane, tetracyclododecane, and hexacyclopentadecane are unstable at the temperatures and pressures typical of CVD diamond growth. Instead, Angus et al. [96, 97] suggested that fully hydrogenated ring compounds structurally related to the boat-boat conformer of bicyclodecane are more plausible nucleation seeds, due to

their greater abundance in CVD systems, thermodynamic stability, and higher reactivity with hydrocarbon radicals leading to atom addition.

While dilute concentrations of 50–200 nm diamond crystals have been successfully produced via homogeneous nucleation using a number of reactant gas mixtures and reactor types [90, 92, 98], it has been found that higher nucleation densities may be achieved when impurities such as halogens, silane, or diborane are present in the system [99]. It has been suggested that, because of the higher rates of thermal dissociation of these impurities, the decomposition fragments quickly nucleate a relatively large number of small clusters. These clusters then serve as seeds for the subsequent addition of carbon.

2. Heterogeneous nucleation

It is possible to grow diamond homoepitaxially on a single crystal diamond surface using methods such as hot-filament CVD [69, 100] and microwave plasma assisted CVD [101, 102] using a variety of hydrocarbon sources. Diamond will readily nucleate on cubic boron nitride (cBN) because the two materials have identical crystal structure, a lattice mismatch that is only 1.4%, and similar thermal expansivity [103, 104]. However, in almost all other diamond CVD processes where diamond is grown on non-diamond substrates, the initial nucleation stage is extremely slow and nucleation density is very low, unless some form of active substrate pretreatment takes place.

Conventional growth of polycrystalline diamond generally consists of up to five distinguishable stages, which are (*i*) the incubation period, (*ii*) three-dimensional nucleation of individual crystallites on the substrate surface, (*iii*) termination of surface nucleation and subsequent three-dimensional growth of individual crystallites, (*iv*) faceting and merging with neighboring crystallites, and (*v*) growth of the continuous film. These different stages are illustrated by the micrographs shown in Fig. 7. Before nucleation begins, the system undergoes an incubation period which may last from a period of several minutes up to hours [13, 105], depending upon substrate material, surface pretreatment, and deposition conditions. The lone nano-crystals formed during

the nucleation stage often exhibit roughly spherical geometry. Nucleation density increases with time up to values that, again, depend upon the substrate and pretreatment method, after which surface nucleation ceases to occur at a measurable rate. The isolated crystallites grow and develop faceting due to the relatively high rate of surface carbon diffusion from the surrounding substrate surface. Once the crystals grow large enough to impinge upon one another, they form grain boundaries and then continue growing as a continuous film, as indicated by the highly textured morphology shown in Fig. 7(f).

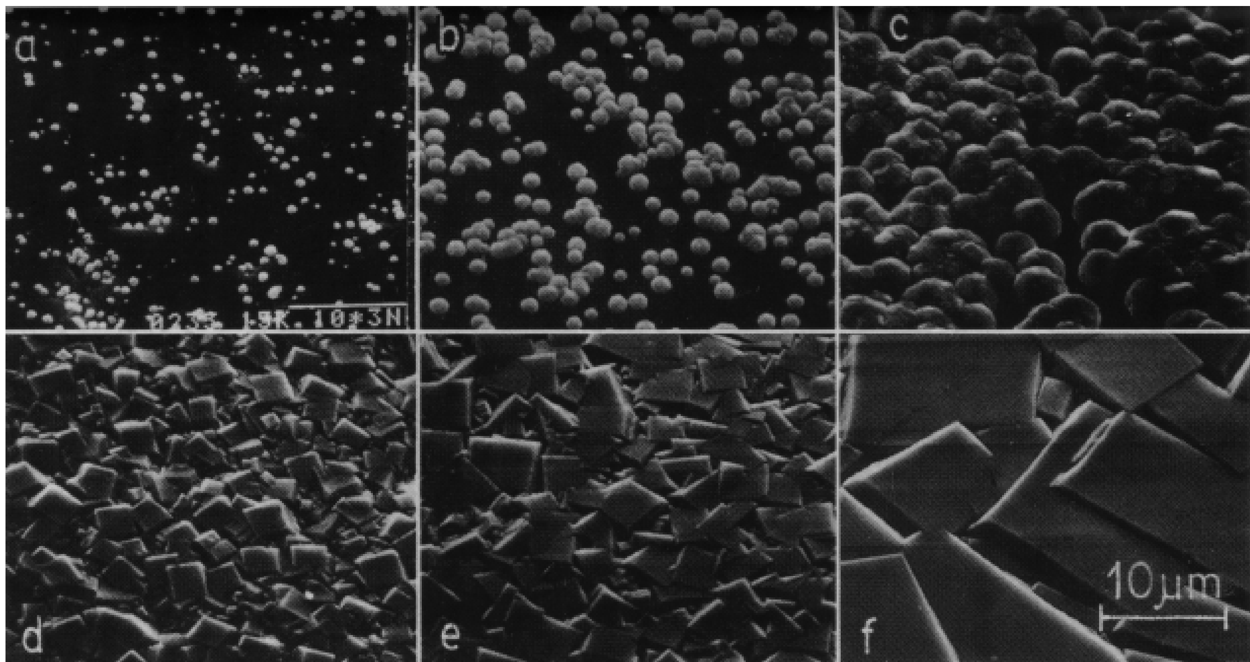

Figure 7. Diamond growth on a non-diamond substrate occurs by sequential steps: (*a*) nucleation of individual crystallites; (*b, c*) termination of nucleation followed by growth of individual crystallites; (*d*) faceting and coalescence of crystallites; (*e, f*) competition between growing crystallites and eventual overgrowth to form continuous film [203].

Under certain growth conditions the competitive growth process of the individual crystallites governs the subsequent growth of the continuous film. In these cases, the grains exhibit fastest growth in the direction perpendicular to the substrate, overshadowing any slower-growing neighbors, and forming a continuous film with a very distinct columnar structure [105]. This mode of film growth, where crystallites successfully overshadow their neighbors, has been observed in many vapor deposited materials, and is described as evolutionary selection [106].

Surface nucleation processes can be described with two quantities: the surface nucleation density, N_d (cm^{-2}), and surface nucleation rate, N_r (cm^{-2} h^{-1}). The nucleation density is the number of nuclei grown per unit area, and the rate is the number grown per unit area per unit time. The density depends upon the number of activated nucleation sites available; thus, nucleation on the substrate will cease when all active sites have been occupied, or when the discrete crystallites grow together and completely cover the surface. The nucleation density determines the ultimate thickness, average crystal size, homogeneity, substrate adhesion, texture, and roughness of the resulting film. Generally, the higher the nucleation density the smoother the surface of the continuous film [107]. On an atomic scale, the surface nucleation process may include the following events:

1. Atoms from the gas collide with the deposition surface and are adsorbed.
2. The adatoms may desorb back into the gas phase or diffuse along the surface; they may also diffuse into the substrate or form bonds with other surface species.
3. As time increases, the concentration of surface adatoms also increases and clusters begin to form as the adatoms bond with one another.
4. The clusters grow or decay in size, depending upon their thermodynamic stability, rate of atom addition from the gas phase, and surface diffusion from the surrounding substrate.
5. Once the clusters reach a critical size, they become thermodynamically stable and will continue to grow as new atoms are adsorbed.

This model for nucleation is necessarily simplistic, because it presumes an ideal substrate with no defects or existing impurities. In practical systems where pretreatment occurs, as discussed in Section IV.C, nucleation may take place on existing particles, at defects induced on the substrate surface, or at intermediate carbide layers of varying chemical composition. However, the general steps outlined above are adequate to describe the principle features of diamond nucleation.

It was recognized fairly early in diamond CVD research that the surface nucleation process of diamond was a controlling factor in the formation and subsequent growth of continuous films [108, 109]. Experiments were performed to nucleate diamond on non-diamond substrates, in-

cluding single- and poly-crystalline Au, Cu, Si, Mo, and W. From those studies, a number of general trends emerged regarding diamond nucleation on non-diamond substrates:

1. Diamond nucleation rates on non-diamond substrates range from $10^3 - 10^8$ cm^{-2} h^{-1}, depending upon the surface preparation method and deposition conditions.
2. Nucleation of the diamond crystals is observed primarily on substrate defects (scratches, grain boundaries, dislocations), indicating that diamond nucleation is, indeed, occurring via a heterogeneous mechanism.
3. Diamond nucleation rates are lower on single-crystal substrates than on polycrystalline substrates of the same material after identical surface pretreatment.
4. Diamond nucleation rates on carbide-forming substrates (Si, Mo, W) are one to two orders of magnitude higher than on non-carbide-forming materials (Cu, Au).
5. Nucleation rates on non-diamond substrates decrease as both substrate coverage and crystal size increase.

A large number of experimental observations employing transmission electron microscopy, scanning electron microscopy, x-ray diffraction, x-ray photoelectron spectroscopy, low-energy electron diffraction, Rutherford backscattering spectrometry, electron energy loss spectroscopy, and Auger electron spectroscopy, to name but several techniques (for example, [110-117]), validate the observations of Spitzyn et al. [108, 109]. Together, the experimental studies of diamond nucleation and growth reveal that, in most cases, diamond does not actually nucleate directly on a non-diamond substrate surface, but instead, forms on an intermediate layer that develops at the interface of the substrate during the incubation period prior to actual diamond nucleation. The intermediate layer, formed due to chemical reactions between activated gas species and the substrate material, may consist of a combination of diamond-like amorphous carbon, metal carbides, or graphite, depending upon substrate pretreatment, the substrate material, and deposition conditions. It is generally agreed that the intermediate layer provides nucleation sites for diamond crystal growth, and thus increases N_d on non-diamond substrates. Knowledge of the details of formation of the inter-

mediate layers may provide a means of controlling the morphology and texture of the resulting diamond films.

Diamond is often grown on materials that form refractory carbides, such as silicon, molybdenum, tantalum, and tungsten, in part because of the availability of these materials and their thermal properties (they can withstand the high temperatures and energy loads associated with diamond deposition), and in part because it was discovered that diamond would nucleate and grow on these materials with little or no pretreatment. It is now generally accepted that the reason for the ease of growth on these materials is the initial formation of a carbide layer which in turn acts as a medium for diamond nucleation. These intermediate layers are thin, often in the range of tens of nanometers, and do not strongly affect the material properties of the grown film. From observation and thermodynamic calculation [118, 119], it has been suggested that diamond nucleation on Si must be preceded by the formation of a β-SiC buffer layer, and that diamond actually nucleates on the surface of the carbide layer. This is supported by a large number of experiments where particles or films of diamond were grown on silicon substrates.

Systematic studies of diamond growth on other carbide-forming materials have also been carried out [120], and the same observation was made, namely that diamond nucleation was preceded by formation of a thin carbide layer. It has been postulated [121] that diamond growth on carbide-forming substrates is initiated by the dissolution of carbon into the substrate material, forming the stable carbide. Diamond nucleation on the carbide then occurs when the surface becomes saturated with adsorbed carbon. In this model, the diffusion of carbon into substrate and on the surface both play key roles in the rate of diamond nucleation. It was found that qualitative features of the model agreed with experimental observation: materials with high carbon diffusivities had the longest incubation period because they required the most time to achieve a carbide layer thick enough for the surface to become saturated with carbon.

However, enough experimental data exist to conclude that, although the formation of carbide interlayers is an important factor for diamond nucleation on carbide-forming substrates, it is probably not the sole mechanism by which nucleation occurs [122]. Intermediate layers of a-C:H

or a-C were found to form on Si and Mo substrates, for example. Graphite interlayers have also been observed on carbide-forming substrates. What can be said is that, in general, formation of interlayers is a necessary step in the spontaneous nucleation processes of diamond on non-diamond substrates, but this alone is not sufficient for nucleation to occur. Two criteria must be satisfied for non-epitaxial surface nucleation when an interlayer is present: (1) carbon saturation of the substrate surface, and (2) presence of high-energy surface sites (unsatisfied valences). Distinctly different interlayers may form on different substrate materials at different rates, and different reactant-gas mixtures or different substrate temperatures may produce different intermediate layers on the same substrate. Low C:H ratios and/or high substrate temperature may favor the formation of carbides, while high C:H ratios and/or low substrate temperature may lead to the formation of a-C or DLC, or even direct nucleation of diamond on the bare substrate surface.

B. Diamond epitaxy and morphology evolution

1. Epitaxy

Diamond films epitaxially deposited on both diamond and cBN single-crystal substrates demonstrate that, under typical low-pressure processing conditions, single-crystal diamond deposition is possible [109, 123]. However, deposition of single-crystal diamond films on substrates other than diamond and cBN is desirable due to the difficulty in obtaining large area single crystals of either of these two materials. Methods for obtaining large area single crystals, or at least highly oriented films, must be developed for large scale electronic applications. Heteroepitaxial growth of diamond has been and will continue to be a major research objective.

The primary difficulty associated with diamond epitaxy is the small number of materials available with suitable crystal structures and lattice constants. Some transition metals and ceramics, such as Ni, Cu, Fe, and cBN, constitute the few isostructural materials with sufficiently similar lattice constants (mismatch $< 5\%$). Further, the extremely high surface energies of diamond, ranging from 5.3–9.2 J m^{-2} for the principle low index planes, and the presence of interfacial misfit and strain all present major obstacles in forming oriented, two-dimensional diamond nuclei [124].

Early attempts to grow heteroepitaxial diamond on transition metals were unsuccessful, possibly due to the high solubility and mobility of carbon on these materials, and the formation of intermediate layers, as discussed in Section IV.A. More recently, however, there have been a number of successes obtaining heteroepitaxial growth on Ni, Cu, and cBN [104, 124-126].

2. *Oriented growth*

The crystal habit of diamond is, in general, determined by the relative growth velocities of the {100} and {111} planes, denoted as v_{100}/v_{111}, and the appearance or disappearance of crystallographic planes in diamond films depends upon the growth velocities of the corresponding planes. The facets that appear on a crystal are those for which the normal growth velocity is the slowest. Based on the Wulff criterion for crystal habit [127], it is predicted that the most stable growth planes in diamond are the octahedral {111} planes, followed by cubic {100} planes and the {110} planes. At low substrate temperature, when $v_{100}/v_{111} > \sqrt{3}$, the crystal habit of diamond is octahedral, and at high substrate temperature, $v_{100}/v_{111} \leq \sqrt{3}/3$, it is cubic, and in between it is cubo-octahedral. Increasing the hydrocarbon concentration in the gas phase has the same effect as increasing the substrate temperature, specifically, that the morphology of polycrystalline diamond films evolves from octahedral, to cubo-octahedral, to cubic.

Recent success in growing highly oriented, textured diamond on silicon represents a novel approach for obtaining near-single-crystal morphology over large areas [128, 129]. In initial experiments, no texture formed, in part because of the creation of a-SiC interlayers, which led to the growth of randomly oriented diamond particles. Subsequent attempts resulted in the growth of highly oriented, textured films on single crystal Si{100} substrates. In the latter experiments, a two step procedure was applied. First, diamond was nucleated using a CH_4/H_2 gas mixture, and it is believed that *in situ* carburization occurred during this stage, converting the Si surface to an epitaxial β-SiC layer. Nucleation of diamond produced partially oriented nuclei. Then, during the growth stage CO was added to the CH_4/H_2 mixture, resulting in textured growth.

The ability to obtain highly oriented, textured films has led to the investigation of the dependence of film texture and morphology on deposition conditions [130]. Oriented films are categorized according to whether they are (*a*) strongly fiber-textured, (*b*) epitaxially textured films grown on {100} Si, or (*c*) homoepitaxial films grown on {100} diamond. The {100} faceted surfaces were selected because CVD diamond grown on {100} is known to contain significantly fewer structural defects than that grown on {111}. The data for the experiments of Wild et al. [130] were correlated by a growth parameter, $\alpha = \sqrt{3}\left(v_{100}/v_{111}\right)$, and it was concluded that the microstructure (texture and orientation) and morphology of diamond films could be controlled through manipulation of this parameter, which in turn can be controlled by altering the growth environment. For fiber-texture films, low CH_4 concentrations or high substrate temperatures (corresponding to $\alpha <$ 1.5), result in films with a pronounced $\langle 110 \rangle$ texture; at intermediate CH_4 concentrations and substrate temperatures ($1.5 \leq \alpha \leq 3$), a transition of the fiber axis from $\langle 110 \rangle$ to $\langle 100 \rangle$ occurs; further increases in CH_4 concentration or lower substrate temperature ($\alpha > 3$) leads to a complete deterioration of the film morphology, such that the films lose their $\langle 100 \rangle$ texture, and become very fine-grained and do not show any distinct faceting. The evolution of crystal shape as a function of α is illustrated in Fig. 8. In that figure, the arrows indicate the direction of fastest growth.

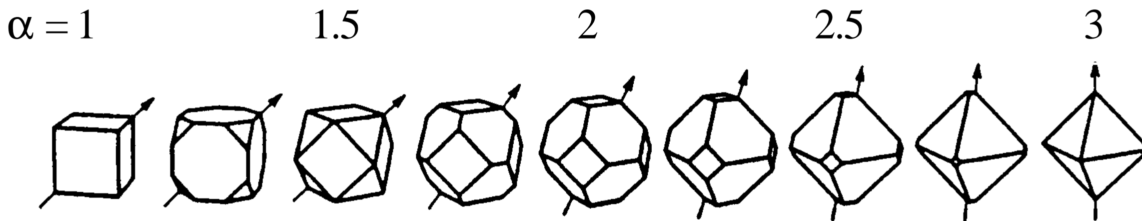

Figure 8. Transition of crystal shape from cubic to octahedral as the growth parameter, α, is increased. The arrows indicated the direction of fastest growth.

In the case of homoepitaxial or heteroepitaxially textured films of {100} orientation, the microstructure and morphology of the films are strongly affected by twin formation, which may lead to complete deterioration of the epitaxial orientation. Deposition conditions corresponding to values of the growth parameter $\alpha \approx 2.5$ tend to suppress twin formation, and the subsequent film growth

improves epitaxial alignment of the crystals. In contrast, small values of the growth parameter ($\alpha \approx 1.5$) usually indicate that the film orientation and morphology will deteriorate due to twinning. The fact that film texture and morphology can be correlated to this one parameter (α) is a strong indication that these two properties depend most strongly on substrate temperature and the gas composition near the deposition surface. By investigating different combinations of T_s and reactant composition, it may therefore be possible to control film texture, surface morphology, and stability with respect to twin formation, and in particular, to grow $\langle 100 \rangle$ textured diamond films with $\{100\}$ faceted surfaces.

3. Morphology evolution

Regarding the size distribution and grain evolution during film growth, a number of experiments indicate that, for nucleation and growth on Si$\{100\}$, the crystal size and size spectrum both grow with increasing deposition time. During the early stages of growth, crystals are small and relatively uniform in size; as the films grow, the average size increases and, simultaneously, the size distribution broadens.

The great disparity in crystal sizes and pronounced surface roughness in high-growth-rate systems led to a detailed set of experiments to study possible morphological instabilities during diamond growth [85]. Indeed, it was observed that in low pressure, high-growth-rate systems (plasma arcjet and combustion), the lack of surface diffusion and re-evaporation at diamond film surfaces during growth accelerated any stochastic interface perturbations, leading to fast growth of some crystals relative to others. The instabilities are then magnified during sustained growth as a result of competitive shadowing and reactant depletion by the taller crystals. This phenomenon is usually only observed in high-growth-rate systems, and only for films thicker than 20 μm. The possible morphological instabilities inherent to diamond film growth not only result in extreme variations in the sizes of the crystallites, but also lead to the incorporation of voids and non-crystalline phases in the films. As growth proceeds, smaller crystals are often found to be coated with DLC, which may be attributed to reactant starvation and lower temperature experienced by

these smaller grains. Several possibilities exist for surmounting these instabilities in high-growth-rate systems. The first is to increase the nucleation density of diamond on the substrate, so that the inevitable onset of instability is delayed. The second is to grow the films in a cyclical manner, so that the growth phase is interrupted regularly with a renucleation phase.

C. Effects of surface conditions

It has long been recognized in film deposition that the substrate material and surface pretreatment both strongly affect the properties of the resulting film. As mentioned above two key issues in diamond deposition are the surface nucleation density and rate, and a number of nucleation enhancement techniques have been developed to maximize both of these quantities. Nucleation density has been increased from less than 10^5 cm^{-2} on untreated substrates up to 10^{11} cm^{-2} on scratched or biased surfaces. The effects of surface conditions on nucleation processes have been investigated to provide guidelines for selection of optimal surface pretreatment methods.

Methods of substrate surface pretreatment that have been tested include (1) scratching with abrasives; (2) seeding with diamond grit and other ceramic powders; (3) electrical bias; (4) covering the substrate with graphite films or fibers; (5) coating the substrate with thin metal films, a-C, C_{70}, cBN, SiC, WC, or hydrocarbon oil; (6) ion implantation; (7) pulsed-laser irradiation; (8) carburization; and (9) chemical etching. These different methods make it possible to control diamond nucleation density over many orders of magnitude.

The reverse problem, that is, preventing diamond from growing on specific portions of a deposition substrate, is important for selective or patterned growth, a technique of particular importance in electronics applications. A number of surface pretreatment methods have been proposed for preventing diamond nucleation on foreign surfaces, including oxidation, sputtering, reactive ion etching, excimer laser irradiation, and surface melting with lasers. It is generally accepted that native oxides (SiO_2) are the most effective at impeding diamond nucleation [131, 132]. Chemical etching in HNO_3, HF, and HCl, plasma etching in NF_3 and Cl_2, and sputtering in N_2

have shown success in introducing surface roughness on selected regions of the surface, but have not resulted in increased nucleation density, and have, in fact, had the opposite effect.

Scratching is the most widely used technique for enhancing diamond nucleation, although this pretreatment method is not easily applied to surfaces of complex shape, and is not generally attempted when growing films that require extremely smooth surfaces. Often in this technique, the surface is scratched, abraded, or blasted with diamond particles or paste, but other abrasives are also used; these include borides, carbides, nitrides, silicides, oxides, and graphite. Diamond nucleation densities after scratching pretreatment typically range from 10^6 to 10^{10} cm^{-2}. Scratching may also be accomplished using ultrasonic vibration with an abrasive paste suspended in methanol or acetone. It has been observed that an ultrasonically damaged surface has more uniformly distributed defects, and this leads to slightly higher nucleation densities (10^7–10^{11} cm^{-2}) and more reproducible effects [99, 122].

A number of explanations have been put forth for the enhancement of nucleation density and rate caused by scratching. The first of these is the seeding effect: diamond, DLC, or other carbonaceous residues from the scratching process are left behind, either adhering to, or imbedded in the substrate, and these nano- and micro-particles may act as nucleation sites [133]. Since other abrasive materials yield a similar, yet less pronounced effect, it is likely that this is not the only operative mechanism in diamond nucleation on scratched surfaces. A second possible mechanism for nucleation is that the highly disordered surface materials or microscopic crater edge sites on the polished surface create high energy sites. Diamond nucleates preferentially at these sites because (*i*) there is a resultant minimization of interfacial energy from the formation of diamond nuclei on the sharp convex surfaces; (*ii*) the microscopic craters and trenches formed by scratching may leave dangling bonds; and (*iii*) carbon saturation will occur most rapidly at sharp edges. Topography patterning analyses lend credence to the second postulate [134]. It was observed that, although residual abrasive powder may enhance nucleation, the nucleation event is promoted by topological features alone, and the presence of residual abrasive is not a necessary condition for nucleation. A third possible mechanism for nucleation is that the scratching process produces non-volatile

graphitic particles through local pyrolysis; the graphitic particles are subsequently hydrogenated in the growth environment.

Scratching and seeding cause substrate surface damage and contamination, as mentioned earlier. Therefore, these pretreatment methods are incompatible with many applications requiring extremely smooth, clean surfaces, such as diamond films for electronic devices, optical window materials, and smooth, wear-resistant coatings. Alternative pretreatment methods that yield high nucleation densities without substrate damage are of particular importance. Biasing pretreatment of substrates has been increasingly employed to enhance surface nucleation of diamond [129, 135, 136]. Using a potential bias to obtain large nucleation densities on unscratched substrates provides an opportunity to control nucleation densities through variation of the applied voltage and current, while reducing surface damage.

Most investigations of bias-enhanced nucleation have focused on mirror-polished Si substrates, and possible explanations for the nucleation enhancement have emerged. For negative biasing of a Si substrate, the role of biasing is to (*i*) increase the flux of carbon-containing cations (C^+, CH_x^+, $C_xH_y^+$) to the surface, expediting the local carbon saturation on the surface and leading to a thin layer of amorphous carbon on the SiC interlayer to form small clusters for diamond nucleation; (*ii*) transfer more energy to the surface through ion bombardment, resulting in increased surface mobility of adsorbed species; (*iii*) reduce and suppress surface oxide formation, and remove native oxides; and (*iv*) accelerate gas-phase reactions because of the increased ion-neutral collisions and higher energy of the sheath region, leading to higher concentrations of reactive hydrocarbon radical species. It is believed that nucleation enhancement on positively biased substrates is due to a high electron density, which in turn results in a high electron kinetic energy. Such high-speed electron impingement process may increase the rate of decomposition of adsorbed hydrocarbons through hydrogen desorption.

D. Effects of deposition conditions

Deposition conditions, such as substrate temperature, reactor pressure, and reactant composition, critically influence diamond nucleation rate and density, but conditions optimal for growth may not be ideal for nucleation. Experiments on bias-enhanced nucleation revealed that negative biasing greatly increases diamond nucleation, but poor quality films are produced when biasing continues during growth [137]. Similarly, optimal values of temperature and pressure for growth may not be the same as those for nucleation.

1. Substrate temperature

Experiments carried out in different reactor systems present a consistent physical picture of the dependence of nucleation density on substrate temperature [138-140]. In these studies it was found that, for growth on silicon substrates, nucleation density falls-off sharply for substrate temperatures below 820–850 ˚C; for temperatures greater than 850 ˚C, the nucleation density gradually decreases but remains on the order of 10^{10} cm^{-2} up to the highest temperatures studied (950 ˚C). It is speculated that this overall dependence of nucleation density on substrate temperature is due to the change in adsorption state and surface diffusion length of growth precursors. At temperatures below approximately 900 ˚C, the nucleation precursors are adsorbed primarily by physical adsorption (physisorption), while chemical adsorption (chemisorption) is dominant at higher temperatures. This change in the adsorption state causes an abrupt change in the diffusion length of the precursors as the temperature is increased above 900 ˚C. As a result, the capture efficiency of precursors on the substrate surface, and thus the nucleation rate and density, dramatically increase when the temperature approaches 900 ˚C.

2. Reactor pressure

Investigations indicate that there is an inverse relationship between pressure and nucleation density and rate, at least for diamond growth on silicon [111, 141]. However, the effect does not appear to be nearly as strong as substrate temperature, resulting in a factor of 3–4 decrease when

the pressure is increased from 2 to 50 Torr. For silicon substrates, it is possible that the inverse dependence on pressure is due to a competition effect between β-SiC formation (which increases diamond nucleation density), and atomic hydrogen etching of material, which decreases the number of nucleation sites. Because of these observations it has been suggested that the nucleation phase be carried out at lower pressure (2–5 Torr), and subsequent growth be carried out at higher pressure (20–40 Torr).

The effect of pressure has also been examined for nucleation on Mo substrates [142]. It was found that good nucleation density was achieved for high gas-phase hydrocarbon fractions at low pressure due to the promotion of carburization of the substrate surface and increased surface C concentration. Growth was then carried out at lower hydrocarbon concentrations and higher pressure to preserve diamond film quality. Films grown in this manner have been shown to be dense, homogeneous, and well-crystallized.

3. Reactant composition

In nucleation on carbide-forming substrates, it has been observed that diamond nucleation density increases as the inlet CH_4 mole fraction is increased. The gas composition influences not only the nucleation density, but also the nucleation behavior and the resultant crystal morphology. At lower CH_4 mole fractions ($< 0.5\%$), diamond nucleation may actually cease while a significant area of the substrate remains unnucleated, and the subsequent growth leads to good-quality, well-faceted, isolated diamond crystals. At higher CH_4 concentrations (1–2%), isolated crystals may grow large enough to occlude one another before nucleation terminates [143]. A side effect of higher hydrocarbon concentrations is formation of appreciable non-diamond components.

The addition of small amounts of oxygen has been generally found to reduce the incubation period and to increase nucleation density. For growth on silicon, it has been postulated that the role of oxygen is to participate in reactions leading to preferential formation of SiO_x on the surface rather than SiC; the SiO_x layer may impede Si diffusion from the bulk to the substrate surface, allowing the adsorbing carbon species to saturate the surface more quickly and then nucleate [144].

Further, the presence of oxygen allows for lower substrate temperatures during nucleation due to the lower binding energy of OH to C (3.68 eV) compared to that of CH to C (4.63 eV); OH is more readily abstracted by atomic hydrogen, creating reactive sites for hydrocarbon adsorption.

However, for growth on Ni and Pt substrates, oxygen may have an adverse effect. In experiments using these substrate materials it was observed that, although the addition of oxygen did not suppress growth of existing diamond and resulted in sharply faceted crystals, it degraded diamond nucleation by eliminating nucleation sites [114]. For high oxygen concentrations (O:H = 1), Ni and Pt surfaces are etched clean; oxygen must be decreased by a factor of 2 or more (O:H $\leq$ 0.5) before nucleation sites last long enough for growth to occur. Once growth does occur, oxygen does not act as an inhibitor, and, in fact, the reason that large, well-faceted crystals form is due to the preferential etching of potential nucleation sites on the crystals, thereby suppressing secondary nucleation.

V. In situ diagnostics

The rate of growth of a diamond film and its uniformity, morphology, texture, and thermal and mechanical properties all critically depend upon the state of the gas phase adjacent to the deposition surface, that is, the composition, temperature, and flow field. The gas properties at the surface, in turn, depend upon the upstream conditions in the reactor. As discussed in Section VI, one- and two-dimensional physical models have been used, with varying degrees of success, to predict the flow field, and temperature and species profiles within different types of diamond CVD reactors. Such models are a powerful tool for exploring issues related to diamond growth, and may help provide links between operating conditions and film growth rate, morphology, and quality. However, the models cannot stand alone: to gain a true understanding of the mechanisms underlying diamond growth it is necessary to couple predictions with experimental measurement. *In situ* measurements of the gas phase and the deposition surface during diamond growth provide data that may be used both as input to the detailed models and as a means of validating such models. Diagnostic technique may be used, for example, to measure concentrations of postulated growth

precursors such as CH_3 or the species crucial for diamond growth, atomic hydrogen. Because the mechanisms describing the gas-phase chemistry are relatively well understood, it may only be necessary to measure several key species in order to have a quantitative knowledge of the overall species distribution.

A strong need also exists for on-line process monitoring in diamond CVD because this material is extremely expensive to synthesize, and many reliability issues remain to be addressed. Diagnostics well-suited for fundamental studies are not necessarily appropriate as process monitors. Currently, most process measurement and control techniques in diamond reactors focus on average substrate temperature, reactor pressure, reactant flow rate, and power. These are important parameters, but they do not give enough explicit information to uniquely determine the state of the gas phase. For example, if laboratory measurements of gas-phase composition and temperature reveal a strong correlation between specific measurable quantities and film growth rate and/or properties, there may be an opportunity to exploit this information through the development of an on-line process sensor. Such a sensor could be tightly coupled to an overall process control strategy.

Discussion of the diagnostic methods in this Section is segregated according to the reactor type in which the measurement was made: hot-filament, plasma-assisted, and combustion. This Section will not constitute a thorough review of diagnostic techniques employed in diamond CVD but is instead intended to indicate how measurements made by extraction, physical probes and optical probes advance understanding of the growth process. A complete review of gas phase diagnostic techniques in diamond CVD was recently presented by Thorsheim and Butler [145].

A. Hot-filament deposition

The hot-filament reactor is the most studied of the various diamond reactor types. Diagnostics in hot-filament systems have addressed three specific issues: (*i*) identification of diamond growth precursors, (*ii*) determination of the role of other species in the growth process, and (*iii*) quantification of the effect of operating conditions on gas-phase composition and spatial distribution. One

of the first measurements of the gas phase environment in diamond CVD was made by Kawato and Kondo using gas chromatography (GC) to sample residual gas from a reactor [146]. They observed detectable quantities of CH_4, C_2H_4, C_2H_2, H_2, and CO from a feed gas mixture of $CH_4/H_2/O_2/Ar$, and found that most of the inlet CH_4 was converted to C_2H_2. As more oxygen was added to the system, the amount of CO increased at the expense of C_2H_2. Because this was a sampling of the downstream stable gas species, the relationship between the measured concentrations and the conditions at the growth surface is not clear.

Celii et al. [24] used infrared diode laser absorption spectroscopy for the *in situ* measurement of gas species in the region between the filament and the substrate. Using this method, C_2H_2, CH_3, C_2H_4, and CH_4 were detected. In contrast with the measurements of Kawato and Kondo, CH_4 was found to be the predominant species ($\approx 8\times10^{14}$ cm^{-3}), with a concentration approximately four times greater than that of C_2H_2, and a factor of ten greater than CH_3. The fact that the measured CH_4 concentration was over 40% of its inlet value indicates that a significant fraction of the inlet gas may completely bypass the filament, never undergoing thermal or heterogeneous dissociation.

Using a combination of *ex situ* mass spectroscopy and x-ray photoelectron spectroscopy (XPS), Harris et al. [147] investigated diamond growth on platinum. By sampling at discrete points between the filament and the substrate, they observed that only CH_4 showed a significant change with position, with its concentration growing by a factor of five, 30 mm from the filament. The concentrations of C_2H_2 and C_2H_4 remained flat in this region. Wu et al. [148] also used gas chromatography and quartz microprobe sampling through a temperature controlled probe to measure gas-phase concentrations. They found that, while the CH_4 concentration also increases with distance from the filament, the increase was a factor of 3, rather than the factor of 5 reported by Harris et al. [147]; the C_2H_2 mole fraction was seen to decrease by a factor of 2. The discrepancies between the results may be explained by differences in deposition conditions and reactor geometry.

Atomic hydrogen has also been measured in hot-filament reactors using laser induced fluorescence (LIF) [22, 149], and its concentration was inferred from crossed beam coherent anti-Stokes Raman spectroscopy (BOXCARS) measurements of H_2 concentrations [150]. The LIF measurements indicated that, with no substrate present, H concentrations only decreased by a factor of 3 (relative to the value at the filament) at a distance of 30 mm from the filament. This result is expected because the low pressures used in the experiments (20 Torr) greatly reduce the rate at which H recombines to form H_2. The known high reactivity between H and heated surfaces (such as a substrate) would undoubtedly cause a more significant drop in H concentration with distance from the filament if a surface were present. The atomic hydrogen concentrations derived from the BOXCARS measurements [150] were an order or magnitude greater than those obtained from the LIF measurements. The differences between the two measurements were explained by filament temperature variation and other experimental factors. Molecular beam mass spectrometry (MBMS) measurements of predominant gas phase species were made within 0.1 mm of the substrate [15], and it was found that the absolute H concentrations were uniformly lower than those measured by either LIF or BOXCARS. As shown in Fig. 9, the MBMS measurements revealed that, as the inlet CH_4 concentration was varied between 0.4% and 7%, a transition occurred in the predominant hydrocarbon species present near the substrate: C_2H_2 was dominant for CH_4 feed fractions less than ≈1%, while CH_4 was dominant for feed fractions greater than this value. It was postulated that CH_4 became the dominant species near the substrate because the filament became coated with carbonaceous material for high inlet carbon concentrations, and this poisoning resulted in lower atomic hydrogen con-

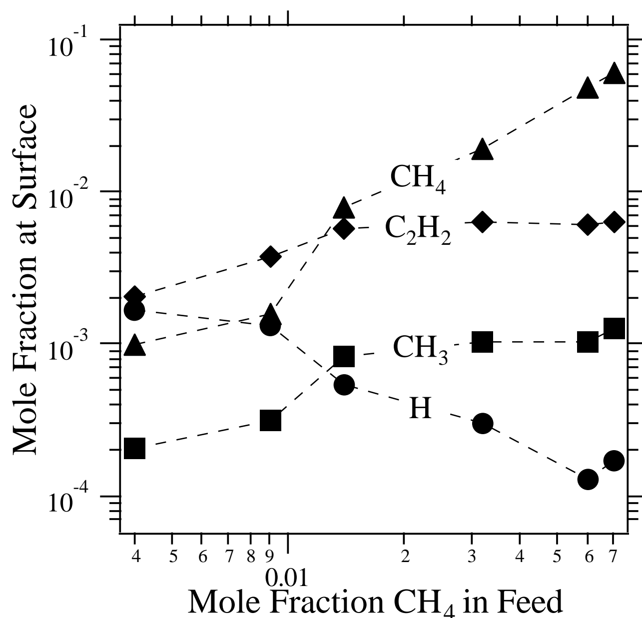

Figure 9. Species mole fractions measured by MBMS sampling at the surface in a hot-filament reactor as a function of methane fraction in the feed gas [15].

centrations and hence lower conversion of CH_4. This was corroborated by a subsequent theoretical study using a stagnation flow model in which a primitive filament poisoning model was included [28], as described in Section VI.A. It was also observed in the MBMS study that, at the surface, CH_3 closely tracked CH_4, and its concentration was approximately 10% that of CH_4, a result consistent with the infrared diode laser measurements of Celii et al. [24].

A possible diamond growth precursor, CH_3, has a much stronger concentration dependence on distance from the substrate than do other measured stable hydrocarbon species such as CH_4, C_2H_2, or C_2H_4, and it is expected that this larger spatial gradient is due to the higher reactivity of CH_3. Resonance-enhanced multiphoton ionization (REMPI) was used to measure CH_3 concentrations 4 mm above the substrate, in a system where the filament-to-substrate distance was varied from 7 mm to 16 mm [151]. The methyl radical concentration was a factor of 3 lower when the separation distance was 7 mm than when it was 16 mm. REMPI was used in a similar reactor system to measure concentrations of CH_3, CH_4, and C_2H_2 at different substrate temperatures [152]. By incorporating the concentration data with measured film growth rates, an apparent activation energy of 0.17 eV in CH_3 concentration was determined, while there were no measurable substrate temperature dependencies observed for CH_4 and C_2H_2. Absolute concentration profiles for CH_3 as a function of distance from the filament were measured [153] using cavity ring-down spectroscopy (CRDS) [154]. A peak in CH_3 concentration was detected several millimeters from the filament, indicating that this species is formed by gas-phase reactions rather than heterogeneous filament chemistry, as shown in Fig. 10. The CH_3 concentration was also observed to increase linearly with susceptor temperature.

Measurements of CH_4 concentrations using CARS [155] and atomic hydrogen using REMPI [25] have shown that, near the filament, the upstream and downstream spatial profiles are the same. In other words, the concentration profiles of CH_4 and H are independent of whether the measurements are made upstream and downstream of the filament. The conclusion to be drawn from this result is that, indeed, mass transport in hot-filament reactors is completely dominated by diffusion, and convection plays a secondary role at best. Models of diamond growth in hot-

filament reactors have confirmed that growth rate is independent of filament-substrate orientation [28, 156].

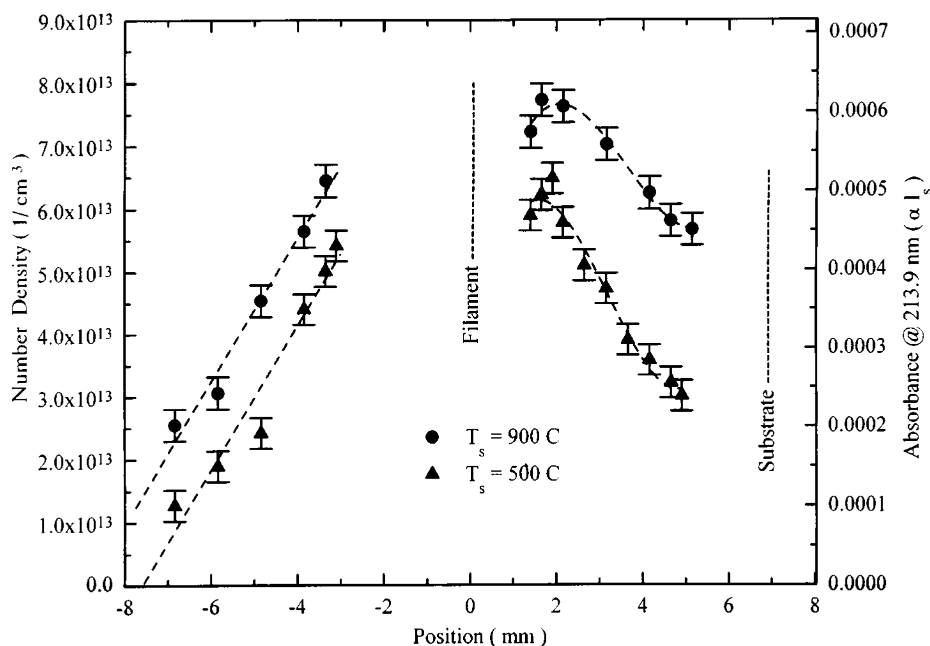

Figure 10. Spatial profiles of CH_3 density and absorbence in a hot-filament reactor at two different susceptor temperatures [153].

Spatial temperature distributions have been measured using thermocouples [14], BOXCARS [150], and LIF [157]. These different experimental techniques consistently show a very sharp temperature drop from the filament to the surrounding gas. For example, LIF temperature measurements showed a drop from 2600 K on the filament to 1400 K 1 mm from the filament, in a reactor operating at 30 Torr. The lower the operating pressure, the more pronounced is the apparent temperature discontinuity between the filament and adjacent gas. As shown in Fig. 11, BOXCARS measurements found that, for a 2870 K filament and 20 Torr operating pressure, the temperature dropped to 2600 K within 0.1 mm of the filament. This effect is well known and was first discussed by Langmuir [18], and is observed in many thermal systems operating at low pressure; the discontinuity is observed within one or two mean-free-paths (75-125 μm at 20 Torr) where continuum heat-transfer theory is not applicable.

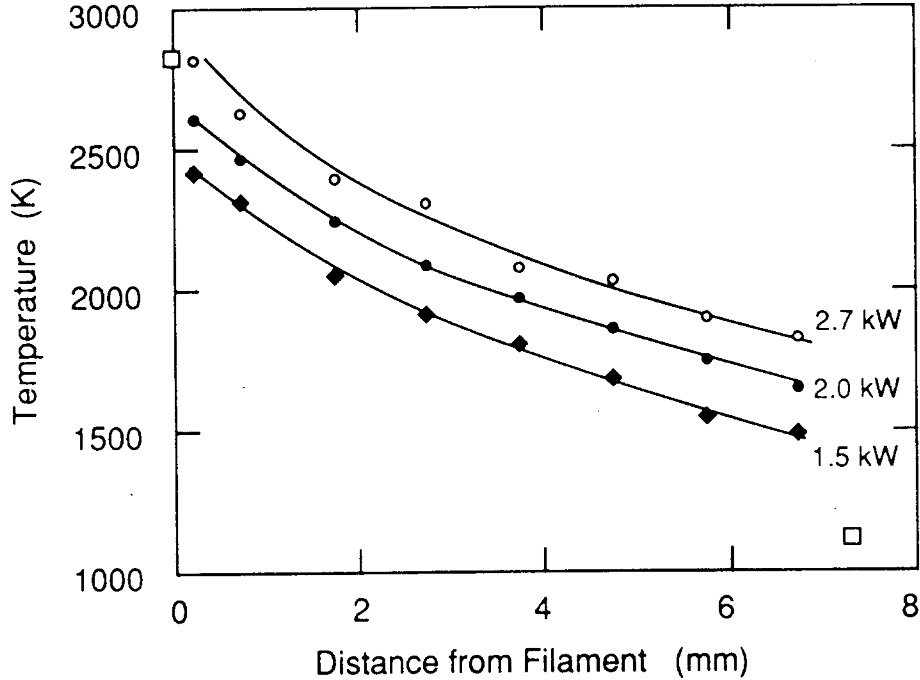

Figure 11. Gas temperature in a hot-filament reactor with 1% CH_4 in H_2, for filament power of 2.7, 2.0, and 1.5 kW. The open squares indicate the filament and substrate temperatures for 2.0 kW filament power [150].

B. Plasma-assisted deposition

A popular technique for determining the composition of plasmas is optical emission spectroscopy (OES). High temperature plasma systems such as dc arcjet show elevated levels of CH and C_2 when compared to systems such as microwave, and these emissions are useful in determining the presence of specific species and for use as a process monitor [158]. The use of OES as a sensor for process control in low-pressure dc arcjet [159] and microwave reactors [160] has been investigated. For the microwave system it was found that there was a linear relationship between C_2, CH, and H(β) emissions throughout the plasma.

Molecular beam mass spectrometry has also been used to determine absolute species concentrations near the substrate in microwave [161] and arcjet [162] plasma reactors. In the 20 Torr microwave system, the effects of hydrocarbon source (CH_4 and C_2H_2), hydrocarbon concentration, and substrate temperature on gas-phase species concentration distribution near the substrate were studied. As illustrated by the data in Fig. 12, over the range of inlet carbon mole fractions considered, the composition near the substrate was independent of the specific source gas, indicating that

the plasma was very efficient at scrambling the species during transport to the substrate. The composition was also found to be insensitive to substrate temperature, so that, although the film growth rate was temperature dependent, the gaseous species are governed by upstream processes that do not depend on the details of the heterogeneous kinetics.

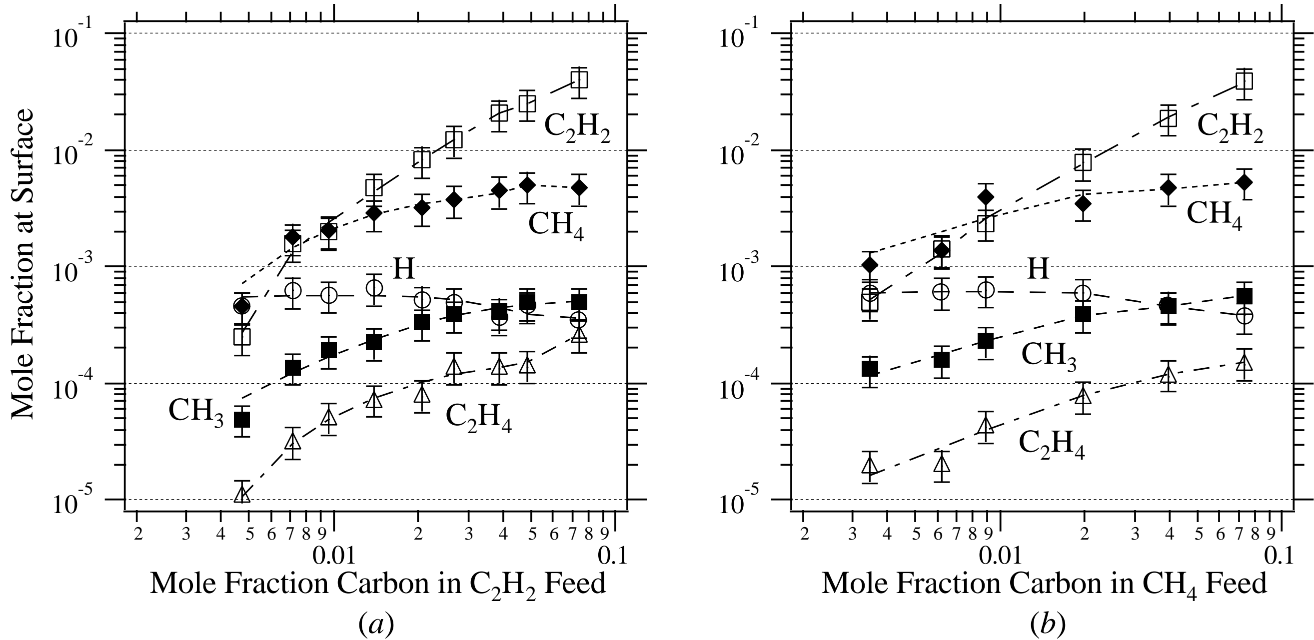

Figure 12. Mole fractions of species measured near the substrate in a microwave reactor as a function of the carbon mole fraction in (*a*) acetylene feed and (*b*) methane feed. Reactor pressure (20 Torr), microwave power (850 W), and substrate temperature (825 ˚C) were held constant [161].

Regardless of the hydrocarbon reactant gas, when the mole fraction of carbon in the feed was less than 1%, CH_4 was the dominant species detected near the substrate, while C_2H_2 was dominant for inlet mole fractions greater than 1%. Atomic hydrogen was found to be relatively insensitive to inlet carbon mole fraction, comprising approximately 0.07% of the gas mixture. In the arcjet study [162], a 1% mixture of CH_4 and H_2 was passed through a 1 kW arc into a 200 Torr reactor. It was found that a significant fraction of the inlet CH_4 was converted to C_2H_2 and C_2H_4, and that the C_2H_2 concentration near the substrate grew approximately linearly with CH_4 flow as the amount of CH_4 in H_2 was raised from 0.3% to 1.5%. Attempts were made to measure CH_3 in that work, but it proved impossible to distinguish between actual CH_3 and that produced as a fragmentation product.

Actinometry has been used by a number of investigators to measure the relative ground state concentrations of species, most notably, atomic hydrogen, using Ar as the actinometer [163-165]. It was observed by Mucha et al. [163] that, in CH_4/H_2/He/Ar mixtures, an increase in CH_4 gave rise to a decrease in the H concentration, and the addition of oxygen resulted in an increase in H, possibly due to passivation of the reactor walls. Spatially resolved relative concentrations of atomic hydrogen were measured by Reeve et al. [165] in a dc arcjet reactor using a CH_4/H_2/Ar reactant mixture with no substrate present. It was observed that the H concentration dropped rapidly with distance from the plasma torch exit, reaching a relative value 30% of its initial maximum within 6 cm. The actinometry data, integrated along the line of slight, was found to be in excellent agreement with predictions of a one-dimensional model containing detailed pyrolysis chemistry. One drawback of actinometry, particularly in systems with appreciable electron densities, is the effect of the noble gas on plasma chemistry. Zhu et al. [166] carried out experiments in a microwave system with a CH_4/H_2 plasma, and found that, upon addition of a noble gas, the emission intensity of various species changed, and the magnitude of the effect depended on the specific noble gas species introduced. It was determined that if a noble gas is to be used as an actinometer, its concentration should be kept below 1%. Ground state concentrations of atomic hydrogen have also been measured using third harmonic generation [167, 168]. The amount of atomic hydrogen present was seen to increase with plasma power, while it decreased as CH_4 was added. Another non-linear technique, resonant degenerate four-wave mixing, was used to measure CH and C_2 concentrations and gas temperature within the boundary-layer in a convection-dominated plasma reactor [169]. Measured CH profiles compared well with predictions obtained from a one-dimensional stagnation-point flow model in which the experimentally determined temperature profile was used.

Other work in plasma-assisted systems has been directed at determining concentrations of stable species such as C_2H_2 and CH_4 using Fourier transform infrared spectroscopy (FTIR) in a microwave plasma reactor [170] and CARS in a diffuse rf plasma [155]. The quantitative differences in species' concentrations measured in these two reactor types illustrates important distinctions in the gas-phase chemistry induced by the different energetic sources. In the microwave system, only

C_2H_2 and CH_4 were detected when the hydrocarbon constituted less than 1% of the inlet gas stream, while in the rf plasma no acetylene could be detected for comparable inlet conditions. Based on known detection limits it was deduced that, in the rf system, less than 20% of the inlet CH_4 was converted to C_2H_2. As rf power was increased, the measured concentration of CH_4 decreased, indicating that more gas phase conversion was occurring.

Efforts at measuring temperature in plasma systems have met with partial success. Early measurements using Langmuir probes in an arcjet system operating between 100 and 400 Torr greatly overestimated the local temperature, and this was attributed to the disturbance of the plasma by the probe [171]; OES measurements in that same system gave temperatures that were 35–45% of the values measured by the probe. No substrate was present in that experiment, so it is difficult to extrapolate from the observed results to an actual deposition system. More recently, measurements in a dc arcjet system at 60 Torr using a floating double probe found that electron temperatures ranged from 2.3 eV at the exit of the plasma torch to 0.4 eV in the downstream (near the substrate) and peripheral regions of the plasma [172]. Electron densities in that system ranged from 6×10^{10} cm^{-3} near the plasma torch to 1×10^{9} cm^{-3} in the downstream region, indicating that charged species concentrations were small compared with the 3×10^{17} cm^{-3} mixture number density.

Determination of the gas kinetic temperature using OES of H_2 and CN was carried out by Chu et al. [173]. LIF of CN was used to compare the rotational temperature obtained with OES to the gas kinetic temperature. It was found that the rotational temperature was an accurate measure of the gas kinetic temperature, even at pressures greater than 10 Torr, and it was concluded from this that the rotational distribution is a better choice for temperature measurements than vibrational or electronic populations because of the more rapid thermal equilibration of the rotational population. One of the first detailed analyses of C_2 and CH optical emission in a dc arcjet operating under diamond growth conditions with a CH_4/H_2 mixture was carried out by Raiche and Jeffries [174]. Through examination of emission spectra, they concluded that the emission was likely due to chemiluminescent reactions; discrepancies in temperatures derived from emission spectra (5000 K) and those

obtained from LIF measurements (2100 K) [175] were attributed to lack of thermodynamic equilibration of excited state populations. Rotational and vibrational excitation temperatures were determined in a dc arcjet reactor with a CH_4/H_2/Ar mixture, and a substrate located 1 inch below the exit of the plasma torch [176]. While it was found that temperatures converged at the substrate and that rotational temperatures for C_2 and vibrational temperatures for CH closely tracked the gas temperature, the vibrational temperatures for C_2 and rotational temperatures for CH were anomalously high. Analysis of those results indicated that, in the plasma bulk, emission by CH was produced primarily by chemiluminescent reactions, while C_2 was produced by electron-impact excitation. The general conclusion from that work was that OES of C_2 provided an accurate means of obtaining spatially resolved gas kinetic temperatures.

C. Combustion flame deposition

Optical emission has been used in combustion synthesis to detect species such as CH, C_2, H, and O in one system [177] and OH, CH, and C_2 in another [178]. Yalamanchi and Harshavardham observed that the primary combustion zone displayed the strongest emission from the carbon-bearing species, and the emission intensities of CH, H, and O dropped sharply downstream of this zone, while C_2 emission remained fairly constant. Diamond growth was reported when CH emission was significantly stronger than C_2 emission in the primary combustion zone. Hirose et al. [178] also examined emission from the center of the primary combustion zone, and found that conditions optimal for optically transparent diamond correlated to an increase in OH emission and a decrease in C_2 emission. In subsequent work, emission from C_2 at 510 nm was correlated with diamond growth in a C_2H_2/O_2 flame [179]; as can be seen in Fig. 13, C_2 emission increased with the fuel to oxygen ratio, reaching a maximum when the ratio of the fuel flow rate to the oxygen flow rate was 1.1. This maximum in C_2 emission corresponded to a maximum in the deposition rate. More recently, diamond films were grown using a MAPP/O_2 mixture, and OES from OH, CH, and C_2 were measured [158]. MAPP gas is a mixture of methyl acetylene, propadiene, and liquefied petroleum gas. By examining the relative intensities of the CH and C_2 emissions, it was

found that when the MAPP and oxygen flow rates were manipulated such that the ratio of the C_2 $\Delta\nu = 0$ transition to the CH A-X transition was between 1.2 and 1.6, well-faceted diamond films could be grown.

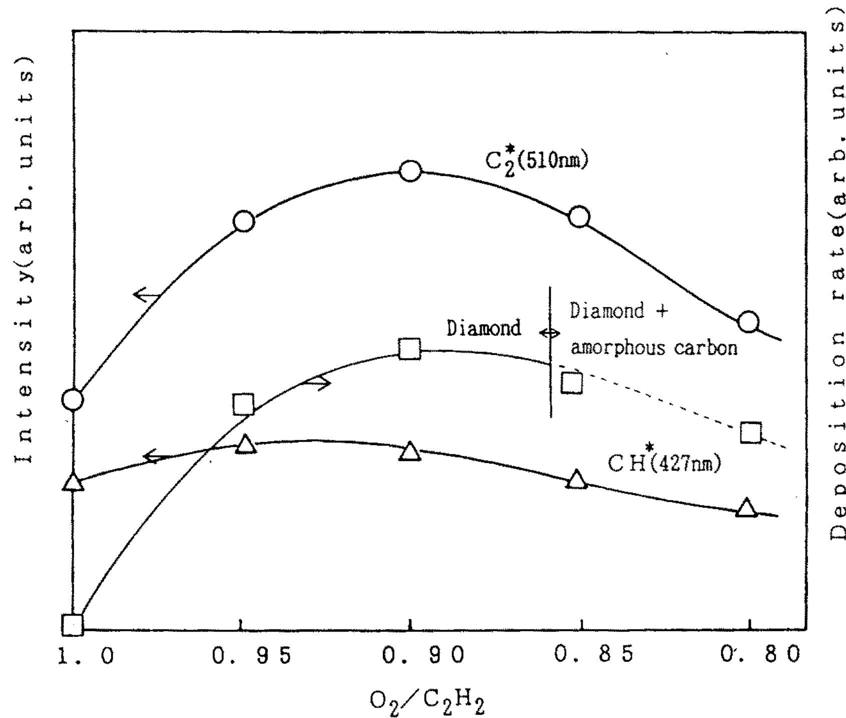

Figiure 13. Emission intensities of C_2 and CH, and deposition rate as a function of stoichiometry in a C_2H_2/O_2 combustion flame reactor [179].

Ground state species have also been measured using LIF and mass spectrometry [180], and GC [181]. The mass spectrometer probe sampled gas from the center of the primary combustion zone; the main gaseous species detected in this region were CO and H_2. Samples taken near the burner showed C_2H_2 and the carbon-bearing radicals to be in near equilibrium. As oxygen flow rate was increased, C_2H_2 concentration decreased near the combustion zone, while H_2 remained nearly constant. The LIF experiments were performed with no substrate present and it was found that maximum OH fluorescence intensities were nearly independent of distance from the combustion zone.

Flame temperature and the concentrations of CO, CO_2, H_2O and OH have been measured during atmospheric-pressure diamond growth using FTIR [182]. Distinct differences in tempera-

ture and composition were observed depending on whether or not a substrate was present; the deposition flame was found to be wider and cooler than the free flame, with the gas temperature lowered by as much as 700 K with the substrate present. In both flames, CO was located primarily in the main combustion zone, while H_2O, CO_2, and OH were found mostly in the outer flame region. A large radial temperature gradient, 700 K/mm, was measured across the diamond growth zone. The steep temperature and composition gradients in many combustion torch systems, such as this one, point to the difficulties inherent in growing large-area, uniform diamond films using combustion synthesis. Obtaining the appropriate gas-phase composition with little or no radial variations points to the need for flat-flame burners and burner-stabilized flames [183-185].

VI. Reactor scale modeling

Numerical and analytical solutions of the governing conservation equations for momentum (fluid flow), mass, and energy (temperature) have led to many insights concerning the mechanisms and conditions under which diamond may be grown by chemical vapor deposition. Modeling many types of diamond reactors has proven successful primarily because the principle hydrocarbon sources used are CH_4 and C_2H_2, and as discussed in Section II, the pyrolysis and combustion mechanisms for these fuels are well understood for the stoichiometries used; and thermodynamic and thermophysical data for the various gaseous species are known. Also, as will be discussed below, the reactor configurations and operating conditions used in dc arcjet, rf plasma, combustion, and hot-filament systems lend themselves to geometric simplifications, which in turn make the numerical models tractable, even with very detailed homogeneous and heterogeneous chemistry. The one-dimensional models of these reactors have proven successful in describing qualitative (species and temperature profile shapes, likely growth precursors) and quantitative (diamond growth rate, species concentrations) features in systems where charged species (plasma) chemistry does not play a significant role. There is a need, however, for more detailed modeling whereby multidimensional effects are captured, and ion-neutral chemistry is considered so that

systems containing non-thermal plasmas, such as microwave reactors, may be adequately described.

A significant factor complicating reactor models is the presence of the energy source. Whether it is the arcjet issuing from a dc plasma torch, the hot-filament(s), or the microwave or rf plasmas, assumptions must invariably be made in constructing a physical model of the source. And, not surprisingly, the particular assumptions strongly affect the predicted temperature and species distributions within the reactor. Because each source type is handled differently, the discussion here is broken up according to reactor type: hot-filament, plasma-assisted, and combustion. Hot-filament is the most studied diamond reactor type, both experimentally and theoretically, and it will be discussed first.

A. Hot-filament reactors

Most of the modeling efforts have focused on determining the temperature profile and, in particular, the species distribution in the region between the filament and substrate to identify likely diamond growth precursors and to develop and validate deposition mechanisms. The models have also been used to examine the role played by the filament in initiating gas-phase chemistry. Theoretical studies of hot-filament reactors may be roughly divided according to whether one- or two-dimensional models were used. The one-dimensional models typically include detailed gas-phase and gas-surface chemistry, and have been used to gain insight into the chemical kinetics governing diamond deposition, and the relationship between mass-transfer and chemistry. Two-dimensional models generally contain limited gas-phase chemistry, and often do not contain deposition mechanisms at all. These models yield information on the details of mass, momentum, and energy transport in reactors.

One of the first detailed studies of the chemistry in a hot-filament system was carried out by Goodwin and Gavillet [186]. It was assumed that the flow between the filament and substrate behaved as an ideal stagnation flow; the gas composition at the filament was determined using homogeneous kinetics and an experimental observation indicating that CH_4 and C_2H_2 were present in

roughly equal concentrations [14]. Figure 14 shows an example calculation of species concentration as a function of height above the substrate from this work. The availability of film growth rate data and the lack of an accepted deposition mechanism led Goodwin and Gavillet to examine the fluxes of individual hydrocarbon species to determine their feasibility as growth precursors. An upper bound, mass transfer limited growth rate of each hydrocarbon species was calculated, and it was calculated that only CH_3, CH_4, and C_2H_2 were present in sufficiently high concentrations at the surface to account for measured growth rates; the conclusion was that one of these three species must be responsible for deposition in the hot-filament environment. This result is consistent with the postulated deposition mechanisms that were being developed, specifically that one or both of CH_3 and C_2H_2 were the species leading to film growth.

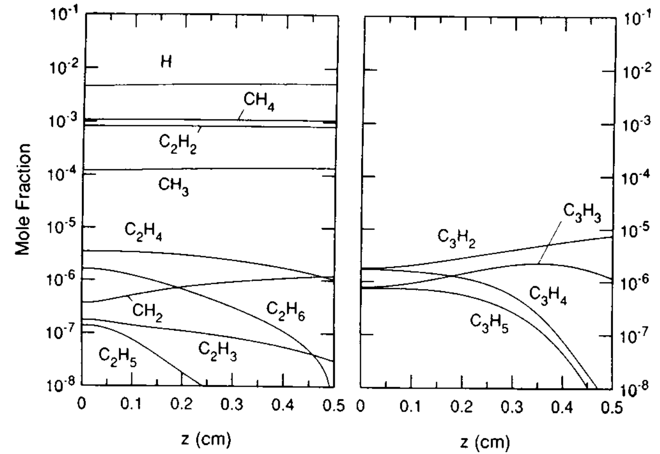

Figure 14. Calculated mole fractions as a function of height above the surface in a hot-filament reactor (for all species greater than 0.1 ppm), from Goodwin and Gavillet [186].

Molecular beam mass spectroscopy data obtained by Hsu in a hot-filament reactor was the first quantitative measure of major species concentrations in a diamond deposition system [15, 187]. By sampling through a pinhole in the center of the substrate, Hsu measured near-surface concentrations of CH_4, C_2H_2, CH_3, and H as a function of inlet CH_4 concentration. (See Section V.A for more discussion of Hsu's experiments.) A modeling study was subsequently carried out to examine Hsu's system [28]. In that work, calculations were performed for H_2-only and CH_4/H_2 feed gases, using a one-dimensional stagnation flow model to describe the region between the filaments and the substrate. For the hydrogen system it was found that, as filament temperature was varied between 1800 K and 2600 K, good agreement with Hsu's data [187] was obtained when (*i*) the H and H_2 near the filament equilibrate around the filament temperature, and (*ii*) the heterogeneous abstraction and termination reactions (1) and (2) were included. The comparison between the ex-

perimental and numerical results is shown in Fig. 15. When the heterogeneous reactions at the surface were not accounted for, atomic hydrogen mole fractions were over-predicted by two orders of magnitude. This result demonstrates the importance of the gas-surface chemistry in determining the gas-phase composition near the surface, and it also demonstrates the significant mass-transfer limitation in hot-filament reactors. That is, the overall kinetic rate of destruction of H by surface reactions is much faster than the rate at which H can be transported to the surface by diffusion. The ratio of these two time scales, diffusion to kinetic, is defined as the Damköhler number (*Da*); for the hot-filament system the effective Damköhler number for atomic hydrogen is on the order of 10–20, depending on conditions, confirming that the system is, indeed, mass-transfer limited.

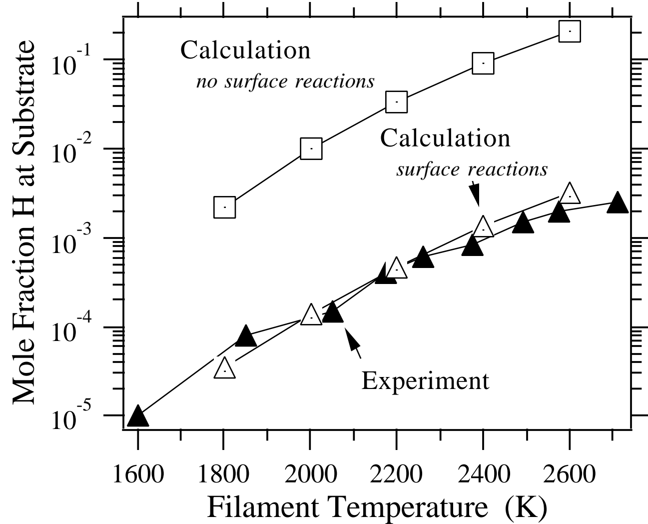

Figure 15. Experimental [187] and theoretical [28] results for near-substrate atomic hydrogen mole fraction in a hot-filament reactor containing only hydrogen.

Numerical results were also calculated for inlet CH_4 concentrations between 0.4% and 7.2% [28]. To obtain good agreement with the experimental data [15] it was necessary to implement a simple filament poisoning model, whereby it was assumed that heterogeneous H_2 dissociation on the filament varied linearly from a maximum when no hydrocarbon was present to a minimum at 7.2% CH_4. The calculated results from that study, together with the measured compositions, are shown in Fig. 16. As can be seen in Figs. 16(a) and 16(b), it was determined that the predicted gas-phase composition did not depend strongly on whether or not a temperature discontinuity between the filament and surrounding gas [150] was used. However, when no filament poisoning was assumed, regardless of the temperature discontinuity, the calculated results for gas composition were in complete disagreement with Hsu's data [15]. The conclusion from the results was that the hydrocarbon blocks reactive sites on the filament surface, and the extent to which sites are

blocked depends on the amount of the hydrocarbon present. Hsu's observation that, to maintain a constant filament temperature, current must decrease as inlet CH_4 increases, confirms this supposition.

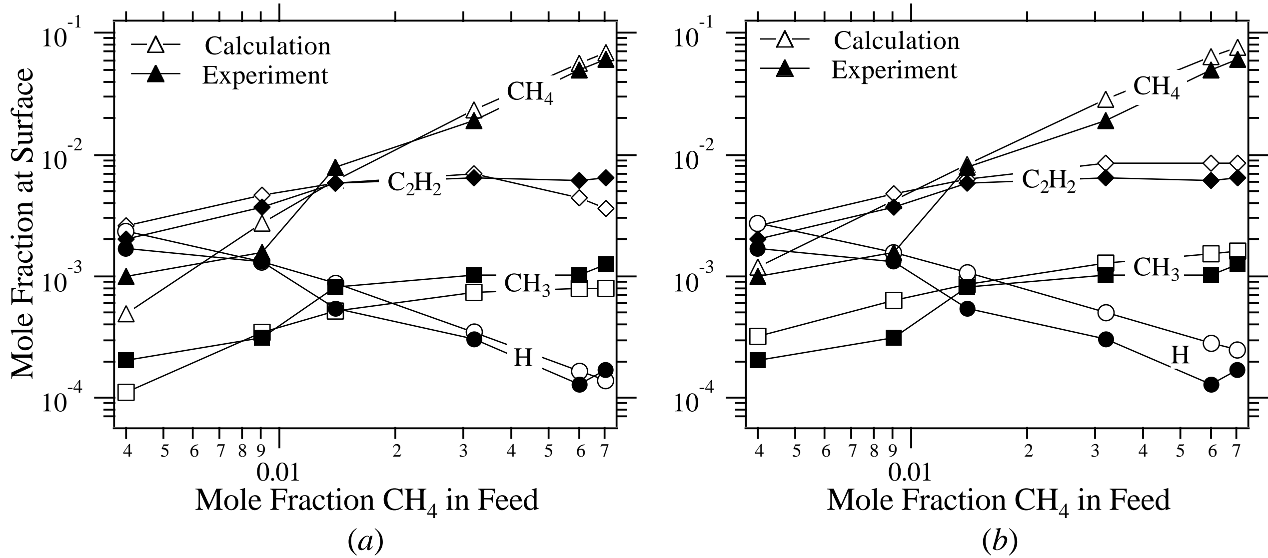

Figure 16. Experimental [15] and theoretical [28] results for gas-phase species distribution at the substrate for a filament temperature of 2620 K and a temperature discontinuity at the filament of (*a*) 900 K, and (*b*) 0 K.

Additional experiments and analyses were carried out to examine the effects of hydrocarbon source (CH_4 versus C_2H_2) and substrate temperature ($255 \leq T_s \leq 825$ °C) on gas composition near the substrate [27]. As with the previous study [28], the numerical model exhibited good qualitative and quantitative agreement with experiment for a variable CH_4/H_2 feed composition and a fixed substrate temperature. For low inlet methane fractions it was predicted that most of this species was converted to C_2H_2, but at higher inlet CH_4 fractions significant conversion did not occur. Agreement between theory and experiment was not as good when the CH_4 feed was replaced by C_2H_2. When the inlet carbon fraction was less than 1%, there was good quantitative agreement, suggesting that the model developed earlier [28] is applicable for C_2H_2 feed when there is little filament poisoning. However, the calculations significantly under-predicted (by as much as 60 times) near-surface CH_3 and CH_4 concentrations at higher inlet C_2H_2 concentrations. The large amounts of CH_4 and CH_3 observed experimentally by McMaster et al. [27] suggest that facile de-

composition of C_2H_2 occurred even when atomic hydrogen concentration was reduced by filament poisoning. The predictions of the model were relatively insensitive to the extent of the poisoning (and hence, the degree of H_2 dissociation), and it is likely that heterogeneous decomposition of C_2H_2 on the filament is the explanation for the discrepancy between the model predictions and the observed data. A discrepancy was also found regarding the dependence of near-surface H concentration on substrate temperature. At low inlet CH_4 fraction (0.4%) and relatively high substrate temperature (825 ˚C), there was good agreement between theory and experiment. But, the one-dimensional calculations indicated that near-substrate H concentration should monotonically increase by almost a factor of 10 as T_s was lowered to 255 ˚C, while the experimental data indicated only a modest rise in H. It was found that by including a simple radial diffusional loss term for H in the model to account for multidimensional effects, the predicted values for H at the substrate were brought into close quantitative agreement with experiment. The effect of substrate temperature on species distribution was also examined [188] for a different set of experimental data discussed in Section V.A [150]. As with the earlier study [27], it was found that the atomic hydrogen concentration was predicted to decrease drastically with increasing substrate temperature. In these calculations, for $600 \leq T_s \leq 1000$ K, the mole fraction of CH_3 at the surface rose by a factor of 5, while for substrate temperatures above 1000 K the CH_3 mole fraction was only weakly dependent on T_s. By examining the predicted CH_3 mole fractions at the surface with and without heterogeneous deposition chemistry, it was computed that for $T_s \leq 950$ K, there was a 14.2 kJ/mol activation energy for CH_3 formation with surface chemistry and a 12.2 kJ/mol activation energy without surface chemistry. It was concluded that the exponential increase in CH_3 mole fraction at the surface with increasing temperature was purely a gas-phase effect and could not be correlated to heterogeneous chemistry.

Multidimensional, that is, two-dimensional and axisymmetric, calculations have been performed by a number of investigators to determine the role of heat and momentum transport in diamond growth, and to relate predicted spatial non-uniformities to film growth rate and thickness variation. One of the first theoretical studies of heat transfer in a hot-filament diamond reactor was

carried out by DebRoy et al. [156]. A vertical reactor was set up in that work and the filament was designed so that axisymmetric behavior could be assumed. It was found that, whether the filament was located above or below the substrate and whether the gases were introduced above or below the substrate, there was little variation in film growth rate. The model predicted the diffusion velocities of important species such as CH_3 and H to be greater than any forced or natural convection velocities, demonstrating that concentration and thermal gradients are primarily responsible for species transport in hot-filament systems. This result has been confirmed by other investigators using one-dimensional models in which the inlet bulk velocity was varied by over an order of magnitude with no measurable effect on near-substrate composition or growth rate [28, 188]. A subsequent study was carried out using the same axisymmetric reactor geometry to examine the effect of atomic hydrogen on heat transfer [189]. It was determined that, for a given filament temperature, the substrate temperature in He was significantly lower than that in either pure H_2 or a 1% CH_4/H_2 mixture, and that small amounts of CH_4 had no appreciable effect on the atomic hydrogen profile. In that work the predicted temperature profiles were in good agreement with measured values. Also, heterogeneous recombination of H was predicted to result in significant substrate heating due to its relatively high flux and the 4.5 eV exothermicity of the net recombination reaction to form H_2.

Because the sole energy source for the gas (and sometimes the substrate) typically consists of, at most, several discrete filaments, work has been done to study the effect of the filaments on substrate temperature uniformity. Wolden et al. [190] calculated temperature profiles in a system consisting of up to three parallel, cylindrical filaments oriented parallel to a silicon substrate in order to determine the relative contributions of radiation, conduction, and convection to substrate heating. It was found that predicted substrate temperature profiles were in reasonable agreement with measured values, and, in agreement with Tankala and DebRoy [189], it was determined that surface H recombination significantly affects absolute substrate temperature. Substrate temperatures were primarily determined by radiation flux, indicating that conduction and convection play secondary roles in the surface heat transfer process. Substrate temperature was predicted to be highest directly

under the filaments, with appreciable gradients in the direction perpendicular to the filament axes. Through numerical experimentation it was found that a two filament configuration could be designed which would yield relatively uniform substrate temperatures.

A two-dimensional model containing a reduced gas-phase kinetic mechanism consisting of 10 species and 12 reactions has recently been developed [191]. Closed-form expressions for heterogeneous H production on the filament and for film growth rate were included in the model. Atomic hydrogen production on the filament was assumed to occur via reactions analogous to (1) and (2), and the relevant kinetic coefficients were adjusted to yield agreement with measured gas-phase H concentrations. At low pressure it was predicted that H production rate on the filament was proportional to H_2 concentration, and this result, coupled with tungsten filament data [192], yielded an H_2 dissociation activation energy of 1.6–1.9 eV for filament temperatures between 2000 ˚C and 2500 ˚C. At higher pressures, H concentrations appear to reach saturation. The two-dimensional reactor model was applied to three different experimental systems [27, 149, 150]. It was found that the temperature discontinuity at the filament had little effect on the results, which is consistent with earlier one-dimensional studies [28, 186]. Also, total carbon near the filament was reduced relative to other regions of the reactor due to thermal diffusion effects. In general, it was concluded that the model adequately predicted the species' concentrations and film growth rates in the different experimental systems.

B. Plasma-assisted reactors

Lack of quantitative data for temperature and composition in dc arcjet reactors has led investigators to use models to predict macroscopic observables such as film growth rate, and to examine near-substrate gas composition for potential growth precursors. Using a modified mechanism with CH_3 as the only growth precursor [59], Goodwin modeled the growth environment of Raiche et al. [34] as a one-dimensional stagnation flow [193]. It was determined that, although there were appreciable concentrations of atomic carbon near the substrate, the growth rate data of Raiche et al. could be adequately reproduced by the modified Harris mechanism. The uncertainty regarding the most probable growth precursor (CH_3 versus C_2H_2) and the predicted high fraction of atomic carbon in dc arcjet systems (because of H supersaturation), led other investigators to propose a mechanism for the deposition of diamond and graphitic carbon, in which all three species—CH_3, C, and C_2H_2—could participate [36]. The mechanism was incorporated into a stagnation flow model for a subatmospheric dc arcjet and used to investigate the dependence of growth rate and graphitic content on the degree of H_2 dissociation and the CH_4 concentration in the feed. It was predicted that CH_3 was the predominant growth species when little of the H_2 in the plasma torch underwent dissociation, and that C became the dominant species at higher dissociation levels. The third growth species, C_2H_2, did not play a role in diamond growth under the conditions considered with less than 1% CH_4 in the feed, but at higher input CH_4 levels, the C and CH_3 incorporation rates where only slightly higher than that of C_2H_2. In a subsequent study [194], the dependence of diamond growth rate on hydrocarbon injector location was modeled. As shown in Fig. 17, it was predicted that, for CH_4 feed, growth rate could be increased by almost a factor of 2 by relocating the injector from a point near the plasma torch exit to just out-

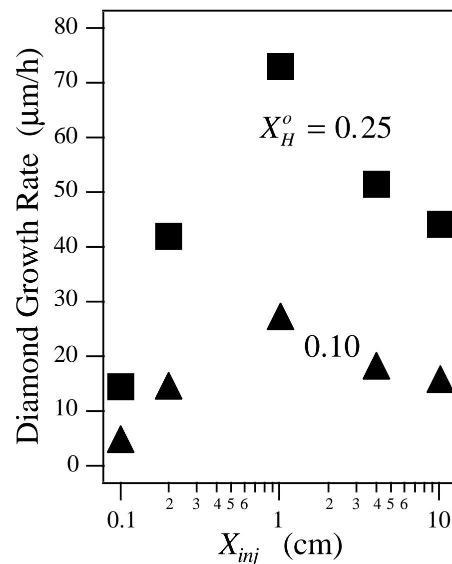

Figure 17. Predicted diamond growth rate as a function of hydrocarbon injector height above the substrate (X_{inj}) in a dc arcjet reactor for two different mole fractions of atomic hydrogen exiting the plasma torch [194].

side the substrate boundary-layer. The growth rate increased as the injector was moved towards the substrate because this increased the near-substrate concentrations of C and CH_3. An experimental study of the effect of injector location was carried out [165], and higher growth rate and improved film quality were observed when the hydrocarbon injector was located near the substrate.

A two-dimensional model of the reacting gas flow, heat transfer, and electrodynamic phenomena in a subatmospheric dc arcjet was recently developed [195, 196]. Reaction rate coefficients for two irreversible reactions describing electron-assisted dissociation of H_2 and CH_4 were obtained in that work by solving the Boltzmann equation for the electron energy distribution function; the coefficients were then used in the gas-phase kinetic mechanism, which consisted of 15 species and 76 reactions. Instead of a detailed deposition mechanism, flux boundary conditions for H and CH_3 were derived in closed form. The model predicted the temperature to peak along the discharge axis (the symmetry axis), and to decay smoothly in the radial direction to the electrodes. The model also predicted the deposition rate, as measured by CH_3 flux, to vary significantly over the substrate surface. Interestingly, the flux non-uniformity was pressure dependent: at 150 Torr it was found that growth rate was minimum at the center, and increased monotonically by over a factor of 2 at a radius of 1 cm. At 75 Torr, however, the growth rate was maximum at the center, and it decreased by a factor of almost 3 at a radius of 0.8 cm, before increasing again at distances greater than this. These results were attributed to the pressure dependence of the CH_3 distribution in the reactor.

Diamond deposition in an atmospheric-pressure rf plasma reactor has also been modeled [197, 198]. A non-reacting (except for hydrogen chemistry), axisymmetric flow model coupled to two-dimensional electromagnetic field equations was used to calculate the velocity and temperature fields in the reactor. The temperature field was then used in a one-dimensional stagnation model to describe the processes occurring within the concentration boundary-layer. The boundary-layer thickness was chosen to lie at the 4000 K isotherm because chemical equilibrium was believed to exist at temperatures above this, that is, in the free stream. In the first study [197] a detailed surface mechanism was not used. Instead, it was assumed that H recombined at the surface to form H_2, and C and C_2 were assigned sticking probabilities of unity. In the second study [198] a detailed

deposition mechanism was developed in which all CH_x species ($x = 0$–3) were possible growth contributors. The predicted growth rate increased strongly as the boundary layer thickness decreased. For relatively thick boundary layers resulting from moderate jet velocities, growth was dominated by CH_3, and for thin boundary-layers growth was dominated by C.

Because of the difficulties involved in modeling non-thermal plasma systems, fewer theoretical studies have been performed on microwave reactors than on dc or rf reactors. As a preliminary step in modeling the two-dimensional (axisymmetric) behavior of microwave reactors, Hyman et al. [38] carried out detailed zero-dimensional calculations by solving the Boltzmann equation to determine the electron energy distribution. This equation was coupled to transient equations describing ion and neutral species chemistry. It was presumed that the simulation modeled the time-dependent reactor behavior at the center of the plasma ball; mass and energy transport effects were accounted for in this zero-dimensional model by including estimates for diffusion and conduction driving forces in the governing species and energy equations. For a reactor pressure of 40 Torr and power deposition of 30 W/cm^3, the model predicted a very rapid electron density buildup for the first several microseconds: it rose from 2×10^9 cm^{-3} at 0.01 μs to 5×10^{11} cm^{-3} at 3 μs, but only increased by another factor of 2 when the time increased to 2 ms. Once the gas reached its equilibrium temperature of ≈ 3000 K after 2 ms, electron processes became unimportant relative to thermal processes in determining the chemical evolution of the gas. Atomic hydrogen concentration also reached equilibrium within 2 ms, constituting over 20% of the neutral gas mixture in a system that initially contained 98.75% H_2, 1% CH_4, and 0.25% O_2. Most of the C1 species reached equilibrium values after approximately 4 ms: CO was the dominant C1 species, at approximately 0.3%, followed by C at 0.2%. Methyl radical was present (at 0.01%), but at lower concentrations than both CH and CH_2. Acetylene was predicted to be present in concentrations comparable to atomic carbon. The appreciable atomic hydrogen concentrations predicted to exist within the plasma ball are considerably higher than those found in laboratory microwave reactors [161], but may be characteristic of the conditions in the commercial ASTeX system being modeled.

C. Combustion reactors

Analysis of combustion flame deposition has focused on the feasibility of using different hydrocarbon fuels, e.g., CH_4, C_2H_2, C_2H_4, MAPP, and determination of the relationship between gas composition and film growth rate. Atmospheric deposition of diamond in premixed $C_2H_2/O_2/H_2$ and CH_4/O_2 strained flames has been modeled using a stagnation flow approximation [199]. Using a lightly sooting combustion mechanism [6] and a 35 reaction deposition mechanism, it was predicted that optimal growth conditions occurred when the burner-to-substrate distance was small, and the flame was lifted from the burner surface and stabilized on the deposition surface. The model was found to be in good agreement with experimental data available for the $C_2H_2/O_2/H_2$ flame [200]. It was also predicted that, because of the high gas velocities, temperatures in the C_2H_2 flame were higher than the theoretical adiabatic flame temperature; it was postulated that the reason for this behavior was the relatively long time required for C_2H_2 to dissociate to its equilibrium concentration. Concentrations of CH_3 near the substrate were high enough in the C_2H_2 flame to account for observed growth rates. In contrast, temperatures in the CH_4/O_2 flame were always lower than the adiabatic flame temperature, and while the gas velocity affected the flame location, it had little effect on peak temperature. In the CH_4 flame, the fractions of CH_3 and H near the substrate were approximately 5 times lower than those produced by the C_2H_2 flame. The bulk of the CH_3 produced in the methane flame never reached the surface; instead, it was rapidly converted to C_2H_2 through bimolecular reactions. It was concluded that, even under optimal conditions, diamond growth rate was considerably lower in atmospheric methane flames than in acetylene flames.

To increase film uniformity, combustion systems are often operated at relatively low pressure [183, 184]. In a combined experimental and theoretical study of diamond growth, films were deposited at 35 Torr to explore conditions that would simultaneously yield moderate growth rates, high film quality, uniformity, and large area coverage [201]. The gas was assumed to behave as an ideal stagnation flow, and the governing equations were coupled to a lightly sooting combustion mechanism [6], and a reduced deposition mechanism in which CH_3 was the growth species, and O and OH acted to abstract surface-bound hydrogen. It was found that the temperature profile pre-

dicted by the model was in close agreement with the profile obtained from OH rotational temperature data, and this was attributed in part to the large postflame reaction zone. Relative OH concentrations were obtained using LIF, and when these were normalized to the theoretical value at a single point (3 mm from the burner), the measured and predicted profiles were in good agreement. It was also found that, when normalizing the experimental OH concentrations, the presence or absence of heterogeneous chemistry in the model had no apparent effect. Because of this, the measured OH concentrations could not be used to evaluate the accuracy of the surface kinetic mechanism.

VII. Summary

This chapter has reviewed the state of understanding of the processes controlling the CVD of diamond. Gas-phase chemistry in this system is understood rather well, owing to much prior work in the combustion community. Much more contentious has been development of a mechanistic view of the elementary surface reactions leading to diamond growth. Indeed, our view is that a number of growth mechanisms and important growth precursor species can be operative depending upon details of the growth environment. Although there is still wide disagreement about the detailed, elementary steps in the deposition process, it appears that CVD diamond growth, and even defect-formation, can be described quite well by reduced models. Such models, although not rigorous in detail, are useful in engineering reactor-scaling studies and process optimization.

Outstanding issues in our understanding of CVD diamond include elementary models for the differing growth rates observed on the different crystal faces of diamond. These different growth rates are key in controlling morphology and crystallite grain structure in polycrystalline diamond [202]. Another area still in need of better understanding is the initiation and control of diamond nucleation on non-diamond substrates. Although the nucleation of diamond has been widely characterized, fundamental and predictive models are still lacking.

Acknowledgments

It is a pleasure to acknowledge financial support of our work on CVD diamond by the Materials Science Program at DARPA, Contract N00014-93-2002, and partial support has also been provided by Texas Instruments. The work performed at Sandia National Laboratories was also supported by the United States Department of Energy under contract number DE-AC04-94AL85000. We have benefited greatly from collaboration and discussions concerning this work with Drs. Richard Woodin, Robert Kee, Ellen Meeks, Wayne Weimer, Wen Hsu, Huimin Liu, James Butler, David Goodwin, and John Angus.

References

1. J. Warnatz, U. Maas and R. W. Dibble, Combustion: Physical and Chemical Fundamentals, Modelling and Simulation, Experiments, Pollutant Formation, Springer, Berlin, p. (1996).
2. J. Warnatz, Combustion Chemistry (J. W. C. Gardiner, ed.), Springer, New York, p. 197 (1984).
3. C. K. Westbrook and W. J. Pitz, Combust. Sci. Technol., 37: 117 (1984).
4. J. A. Miller and C. T. Bowman, Prog. Energy Combust. Sci., 15: 287 (1989).
5. D. L. Baulch, C. J. Lobos, R. A. Cox, C. Esser, P. Frank, T. Just, J. A. Kerr, M. J. Rilling, J. Troe, R. W. Walker and J. Warnatz, J. Phys. Chem. Ref. Data, 21: 411 (1992).
6. J. A. Miller and C. F. Melius, Combust. Flame, 91: 21 (1992).
7. A. Burcat, W. J. Pitz and C. K. Westbrook, "Shock Tube Ignition of Octanes," UCRL - 102001, Preprint (September 27, 1989).
8. C. T. Bowman, R. K. Hanson, D. F. Davidson, W. C. Gardiner, V. Lissianski, G. P. Smith, D. M. Golden, M. Frenklach and M. Goldenberg, "GRI-Mech 2.11," http://www.me.berkeley.edu/gri_mech/
9. M. Frenklach, J. Appl. Phys., 65: 5142 (1989).
10. C. Wolden, K. K. Gleason and J. B. Howard, Combust. Flame, 96: 75 (1994).
11. M. Frenklach and H. Wang, Phys. Rev. B, 43: 1520 (1991).
12. S. J. Harris and A. M. Weiner, J. Appl. Phys., 67: 6520 (1990).
13. S. J. Harris, A. M. Weiner and T. A. Perry, J. Appl. Phys., 70: 1385 (1991).
14. S. J. Harris, A. M. Weiner and T. A. Perry, Appl. Phys. Lett., 53: 1605 (1988).
15. W. L. Hsu, Appl. Phys. Lett., 59: 1427 (1991).
16. I. Langmuir, J. Amer. Chem. Soc, 34: 860 (1912).
17. I. Langmuir, J. Amer. Chem. Soc, 34: 1310 (1912).
18. I. Langmuir, Amer. Chem. Soc., 37: 417 (1915).
19. S. Matsumoto, Y. Sato, M. Tsatsumi and N. Setaka, Jpn. J. Appl. Phys., 21: L183 (1982).
20. S. Matsumoto, Y. Sato, M. Tsatsumi and N. Setaka, J. Mater. Sci., 17: 3106 (1982).
21. F. Jansen, I. Chen and M. A. Machonkin, J. Appl. Phys., 66: 57495755 (1989).
22. U. Meier, K. Kohse-Hoinghaus, L. Schafer and C. Klages, Appl. Optics, 29: 4993 (1990).
23. T. D. Moustakas, J. P. Dismukes, L. Ye, K. R. Walton and J. T. Tiedje, "Polycrystalline Diamond Deposition from Methane-Hydrogen Mixtures," Proceedings of Tenth International Conference on Chemical Vapor Deposition, Honolulu, p. 1164 (1987).
24. F. G. Celii, P. E. Pehrsson, H.-T. Wang and J. E. Butler, Appl. Phys. Lett., 52: 2043 (1988).
25. F. G. Celii and J. E. Butler, Appl. Phys. Lett., 54: 1031 (1989).
26. M. Sommer and F. W. Smith, J. Mater. Res., 5: 2433 (1990).

27. M. C. McMaster, W. L. Hsu, D. S. Dandy and M. E. Coltrin, J. Appl. Phys., 76: 7567 (1994).
28. D. S. Dandy and M. E. Coltrin, J. Appl. Phys., 76: 3102 (1994).
29. F. M. Cerio and W. A. Weimer, Rev. Sci. Instrum., 63: 2065 (1992).
30. R. L. Woodin, L. K. Bigelow and G. L. Cann, Applications of Diamond Films and Related Materials (Y. Tzeng, M. Yoshikawa, M. Murakawa and A. Feldman, ed.), Elsevier Science Publishers B.V., p. 439 (1991).
31. L. Rongzhi, S. Hailiang, Y. Zhen, T. Sen and Z. Hesun, “Transparent Diamond Film Deposited by Optimized DC Arc Plasma Jet,” Proceedings of Applications of Diamond Films and Related Materials, Auburn, AL, p. 207 (1991).
32. D. S. Dandy and M. E. Coltrin, J. Mater. Res., 10: 1993 (1995).
33. N. Koshino, K. Kurihara, M. Kawarada and K. Sasaki, Diamond and Diamond-Like Materials Synthesis (G. H. Johnson, A. R. Badzian and M. W. Geis, ed.), Materials Research Society, Pittsburgh, PA, p. 95 (1988).
34. G. A. Raiche, G. P. Smith and J. B. Jeffries, “Diagnostics of a Diamond-Depositing DC-ARC-Jet Plasma,” Proceedings of New Diamond Science and Technology, Washington, DC, p. 251 (1990).
35. M. H. Loh, J. G. Liebeskind and M. A. Cappelli, “Characterization of a Supersonic Hydrogen Arcjet Plasma Thruster Employed in Diamond Film Synthesis,” Proceedings of 29th Joint Propulsion Conf., Monterey, CA, p. 2227 (1993).
36. M. E. Coltrin and D. S. Dandy, J. Appl. Phys., 74: 5803 (1993).
37. M. H. Loh and M. A. Cappelli, “Study of Precursor Transport During Diamond Synthesis in a Supersonic Flow,” Proceedings of Third International Symposium on Diamond Materials, Honolulu, HI, p. 17 (1993).
38. E. Hyman, K. Tsang, A. Drobot, B. Lane, J. Casey and R. Post, J. Vac. Sci. Technol. A, 12: 1474 (1994).
39. S. P. Mehandru and A. B. Anderson, J. Mater. Res., 5: 2286 (1990).
40. S. P. Mehandru, A. B. Anderson and J. C. Angus, J. Mater. Res., 7: 689 (1992).
41. D. R. Alfonso, S. H. Yang and D. A. Drabold, Phys. Rev. B, 50: 15369 (1994).
42. D. R. Alfonso, S. E. Ulloa and D. W. Brenner, Phys. Rev. B, 49: 4948 (1994).
43. O. F. Sankey, D. J. Niklewsky, D. A. Drabold and J. D. Dow, Phys. Rev. B., 41: 12750 (1990).
44. D. Brenner, Phys. Rev. B, 42: 9458 (1990).
45. J. C. Angus, Z. Li, M. Sunkara, C. Lee, W. Lambrecht, R. L. and B. Segall, “Diamond Nucleation,” Proceedings of Materials Research Society Symposium, Boston, MA, p. 128 (1993).
46. J. Tersoff, Phys. Rev. B, 39: 5566 (1989).
47. W. R. L. Lambrecht, C. H. Lee, B. Segall, J. C. Angus, Z. Li and M. Sunkara, Nature, 364: 607 (1993).
48. N. L. Allinger, J. Amer. Chem. Soc., 99: 8127 (1977).
49. N. L. Allinger, Y. H. Yuh and J. Lii, J. Amer. Chem. Soc., 111: 8551 (1989).

50. S. J. Harris and D. G. Goodwin, J. Phys. Chem., 97: 23 (1993).
51. Y. L. Yang and M. P. D'Evelyn, J. Vac. Sci. Technol. A, 10: 978 (1992).
52. M. Zhu, R. H. Hauge, J. L. Margrave and M. P. D'Evelyn, “Mechanism for Diamond growth on Flat and Stepped Diamond (100) Surfaces,” Proceedings of Third International Symposium on Diamond Materials, Honolulu, HI, p. 138 (1993).
53. D. Huang and M. Frenklach, J. Phys. Chem., 96: 1868 (1992).
54. M. J. S. Dewar and W. J. Theil, J. Amer. Chem. Soc., 99: 4899 (1977).
55. J. Tersoff, Phys. Rev. B., 37: 6991 (1988).
56. D. R. Alfonso and S. E. Ulloa, Phys. Rev. B, 48: 12235 (1993).
57. B. J. Garrison, E. J. Dawnkaski, D. Srivastava and D. W. Brenner, Science, 255: 835 (1992).
58. M. Frenklach and K. E. Spear, J. Mater. Res., 3: 133 (1988).
59. S. J. Harris, Appl. Phys. Lett., 56: 2298 (1990).
60. D. W. Brenner, D. H. Robertson, R. J. Carty, D. Srivastava and B. J. Garrison, Computational Methods in Materials Science (J. E. Mark, M. E. Glicksman and S. P. Marsh, ed.), Materials Research Society, Pittsburgh, PA, p. 255 (1992).
61. S. J. Harris and D. N. Belton, Thin Solid Films, 212: 193 (1992).
62. D. G. Goodwin, J. Appl. Phys., 74: 6888 (1993).
63. L. N. Krasnoperov, I. J. Kalinovski, H. Chu and D. Gutman, J. Phys. Chem., 97: 11787 (1993).
64. S. J. Harris and A. M. Weiner, J. Appl. Phys., 74: 1022 (1993).
65. S. Skokov, B. Weiner and M. Frenklach, J. Phys. Chem., 98: 8 (1994).
66. S. Skokov, B. Weiner and M. Frenklach, J. Phys. Chem., 99: 5616 (1995).
67. M. A. Cappelli and M. H. Loh, Diam. Rel. Mater., 3: 417 (1994).
68. C. J. Chu, M. P. D'Evelyn, R. H. Hauge and J. L. Margrave, J. Appl. Phys., 70: 1695 (1991).
69. M. P. D'Evelyn, C. J. Chu, R. H. Hauge and J. L. Margrave, J. Appl. Phys., 71: 1528 (1992).
70. S. J. Harris and A. M. Weiner, Thin Solid Films, 212: 201 (1992).
71. L. R. Martin and M. W. Hill, J. Mater. Sci. Lett., 9: 621 (1990).
72. C. E. Johnson, W. A. Weimer and F. M. Cerio, J. Mater. Res., 1427 (1992).
73. W. A. Yarbrough, K. Tankala and T. DebRoy, J. Mater. Sci., 7: 379 (1992).
74. S. Skokov, B. Weiner and M. Frenklach, J. Phys. Chem., 98: 7073 (1994).
75. M. Frenklach, S. Skokov and B. Weiner, Nature, 372: 535 (1994).
76. M. R. Pederson, K. A. Jackson and W. E. Pickett, Phys. Rev. B., 44: 3891 (1991).
77. D. Huang and M. Frenklach, J. Phys. Chem., 95: 3692 (1991).
78. J. E. Butler and R. L. Woodin, Phil. Trans. Royal Soc., 342: 209 (1993).

79. T. Tsuno, T. Imai, Y. Nishibayashi, K. Hamada and N. Fujimori, Jpn. J. Appl. Phys., 30: 1063 (1991).

80. H.-G. Busmann, W. Zimmermann-Edling, H. Sprang, H.-J. Guntherodt and I. V. Hertel, Diam. Rel. Mater., 1: 979 (1992).

81. L. F. Sutcu, C. J. Chu, M. S. Thompson, R. H. Hauge, J. L. Margrave and M. P. D'Evelyn, J. Appl. Phys., 71: 5930 (1992).

82. R. E. Thomas, R. A. Rudder and R. J. Markunas, “Thermal Desorption from Hydrogenated Diamond (100) Surfaces,” Proceedings of Second International Symposium on Diamond Materials, Washington, D. C., p. 186 (1991).

83. S. J. Harris and A. M. Weiner, J. Appl. Phys., 75: 5026 (1994).

84. C. Wild, N. Herres and P. Koidl, J. Appl. Phys., 68: 973 (1990).

85. K. V. Ravi, J. Mater. Res., 7: 384 (1992).

86. W. J. P. van Enckevort, G. Janssen, W. Vollenberg, J. J. Schermer, L. J. Giling and M. Seal, Diam. Rel. Mater., 2: 997 (1993).

87. A. Badzian and T. Badzian, “High Temperature Epitaxy of Diamond,” Proceedings of Third International Symposium on Diamond Materials, Honolulu, HI, p. 1060 (1993).

88. M. Frenklach, S. Skokov and B. Weiner, “On the Role of Surface Diffusion in Diamond Growth,” Proceedings of Fourth International Symposium on Diamond Materials, Reno, NV, p. 1 (1995).

89. J. C. Angus and E. A. Evans, “Necleation and Growth Processes During the Chemical Vapor Deposition of Diamond,” Proceedings of Materials Research Society Symposium, Boston, MA, p. 385 (1994).

90. M. Frenklach, R. Kematick, D. Huang, W. Howard, K. E. Spear, A. W. Phelps and R. Koba, J. Appl. Phys., 66: 395 (1989).

91. M. Frenklach, W. Howard, D. Huang, J. Yuan, K. E. Spear and R. Koba, Appl. Phys. Lett., 59: 546 (1991).

92. W. Howard, D. Huang, J. Yuan, M. Frenklach, K. E. Spear, R. Koba and A. W. Phelps, J. Appl. Phys., 68: 1247 (1990).

93. S. Mitura, J. Cryst. Growth, 80: 417 (1987).

94. B. V. Derjaguin and D. V. Fedoseev, Scientific American, 233: 102 (1975).

95. S. Matsumoto and Y. Matsui, J. Mater. Sci., 18: 1785 (1983).

96. J. C. Angus, J. A. Mann, Y. Wang, M. Sunkara, P. A. Washlock, M. Kuczmarski and Z. Li, “Progress Report, DARPA University Research Initiation Grant,” Contract #N00014-89J-3167 (January 31, 1991).

97. J. C. Angus, R. W. Hoffman and P. H. Schmidt, Science and Technology of New Diamond (S. Saito, O. Fukunaga and M. Yoshikawa, ed.), KTK Terra Scientific, Tokyo, p. 9 (1990).

98. P. R. Buerki and S. Leutwyler, J. Appl. Phys., 69: 3739 (1991).

99. G. Popovici and M. A. Prelas, Physica Status Solidi A, 132: 233 (1992).

100. E. Kondoh, K. Tanaka and T. Ohta, J. Appl. Phys., 74: 2030 (1993).

101. S. Katsumata, Jpn. J. Appl. Phys., 31: 3594 (1992).

102. Z. M. Zhang, H. M. Cheng, S. H. Li, Q. Y. Cai, D. L. Ling, S. J. Wang, Z. W. Hu, S. S. Jiang, C. Z. Ge and N. B. Ming, J. Cryst. Growth, 132: 200 (1993).

103. W. P. Chai, Y. S. Gu, M. Li, H. Mai, Q. Z. Li, L. Yuan and S. J. Pang, J. Cryst. Growth, 135: 639 (1994).

104. W. A. Yarbrough, J. Vacuum Sci. Technol. A, 9: 1145 (1991).

105. R. A. Bauer, N. M. Sbrockey and W. E. Brower Jr., J. Mater. Res., 8: 2858 (1993).

106. A. van der Drift, Philips Res. Reports, 22: 267 (1967).

107. B. R. Stoner, B. E. Williams, S. D. Wolter, K. Nishimura and J. T. Glass, J. Mater. Res., 7: 257 (1992).

108. B. V. Spitzyn and B. V. Derjaguin, Problems of Physics and Technology of Wide-Gap Semiconductors (L. L. Bouilov, ed.), Akad. Nauk SSSR, Leningrad, p. 22 (1979).

109. B. V. Spitzyn, L. L. Bouilov and B. V. Derjaguin, J. Cryst. Growth, 52: 219 (1981).

110. C. Trevor, D. Cherns and P. Southworth, "TEM Studies of the Nucleation of CVD Diamond on Silicon," Proceedings of Institute of Physics Electron Microscopy and Analysis Group Conference, Bristol, UK, p. 275 (1991).

111. D. Kim, H. Lee and J. Lee, J. Mater. Res., 28: 6704 (1993).

112. S. M. Kanetkar, A. A. Kulkarni, A. Vaidya, R. D. Vispute, S. B. Ogale, S. T. Kshirsagar and S. C. Purandare, Appl. Phys. Lett., 63: 740 (1993).

113. M. T. McClure, J. A. von Windheim, J. T. Glass and J. T. Prater, Diam. Related Mater., 3: 239 (1994).

114. D. N. Belton and S. J. Schmieg, Thin Solid Films, 212: 68 (1992).

115. K. Kobayashi, M. Kumagai, S. Karasawa, T. Watanabe and F. Togashi, J. Cryst. Growth, 128: 408 (1993).

116. G. A. Hirata, L. Cota-Araiza, M. Avalos-Borja, M. H. Farias, O. Contreras and Y. Matsumoto, J. Phys., 5: 305 (1993).

117. B. Y. Lin, C. P. Beetz, D. W. Brown and B. A. Lincoln, "The Influence of Diamond Surface Perfection on the Preferential Nucleation of sp^2 Carbon during Methane Pyrolysis," Proceedings of Evolution of Surface and Thin Film Microstructure Symposium, Pittsburgh, PA, p. 705 (1993).

118. A. R. Badzian and T. Badzian, Surf. Coat. Technol., 36: 283 (1988).

119. J. A. Baglio, B. C. Farnsworth, S. Hankin, C. Sung, J. Hefter and M. Tabasky, Diamond and Diamond-Like Films and Coatings (R. E. Clausing, L. L. Horton, J. C. Angus and P. Koidl, ed.), Plenum Press, New York, p. 635 (1991).

120. P. O. Joffreau, R. Haubner and B. Lux, Int. J. Ref. Hard Mater., 7: 186 (1988).

121. B. Lux and R. Haubner, Diamond and Diamond-Like Films and Coatings (R. E. Clausing, L. L. Horton, J. C. Angus and P. Koidl, ed.), Plenum Press, New York, p. 579 (1991).

122. W. A. Yarbrough and R. Messier, Science, 247: 688 (1990).

123. M. Komori, T. Maki, T. Kim, G. Hou, Y. Sakaguchi, K. Sakuta and T. Kobayashi, Appl. Phys. Lett., 62: 582 (1993).

124. P. C. Yang, W. Zhu and J. T. Glass, J. Mater. Res., 8: 1773 (1993).

125. A. R. Badzian and T. Badzian, Proceedings of Materials Research Society Symposium Proceedings, Boston, MA, p. 339 (1991).
126. J. Narayan, V. P. Godbole and C. W. White, Science, 252: 416 (1991).
127. M. Moore, Ind. Dia. Rev., 2: 67 (1985).
128. S. D. Wolter, B. R. Stoner, J. T. Glass, P. J. Ellis, D. S. Buhaenko, C. E. Jenkins and P. Southworth, Appl. Phys. Lett., 62: 1215 (1993).
129. B. R. Stoner, S. R. Sahaida, J. P. Bade, P. Southworth and P. J. Ellis, J. Mater. Res., 8: 1334 (1993).
130. C. Wild, R. Kohl, N. Herres, W. Müller-Sebert and P. Koidl, Diam. Related Mater., 3: 373 (1994).
131. J. S. Ma, H. Kawarada, T. Yonehara, J. I. Suzuki, J. Wei, Y. Yokota and A. Hiraki, J. Cryst. Growth, 99: 1206 (1990).
132. J. S. Ma, H. Kawarada, T. Yonehara, J. I. Suzuki, J. Wei, Y. Yokota and A. Hiaraki, Appl. Phys. Lett., 55: 1071 (1989).
133. W. A. Yarbrough, Applications of Diamond Films and Related Materials (Y. Tzeng, M. Yoshikawa, M. Murakawa and A. Feldman, ed.), Elsevier Science Publishers, Amsterdam, p. 25 (1991).
134. P. A. Dennig, H. Shiomi, D. A. Stevenson and N. M. Johnson, Thin Solid Films, 212: 63 (1992).
135. A. Sawabe and T. Inuzuka, Thin Solid Films, 137: 189 (1986).
136. M. Katoh, M. Aoki and H. Kawarada, Jpn. J. Appl. Phys., 33: L194 (1994).
137. B. R. Stoner, G. H. M. Ma, S. D. Wolter and J. T. Glass, Phys. Rev. B, 45: 11067 (1992).
138. Y. Hayashi, W. Drawl and R. Messier, Jpn. J. Appl. Phys., 31: L193 (1992).
139. S. Haq, J. A. Savage and D. L. Tunnicliffe, Applications of Diamond Films and Related Materials (Y. Tzeng, M. Yoshikawa, M. Murakawa and A. Feldman, ed.), Elsevier Science Publishers, Amsterdam, p. 405 (1991).
140. J. W. Kim, Y. J. Baik and K. Y. Eun, Applications of Diamond Films and Related Materials (Y. Tzeng, M. Yoshikawa, M. Murakawa and A. Feldman, ed.), Elsevier Science Publishers, Amsterdam, p. 399 (1991).
141. J. J. Chang, D. Mantei, R. Vuppuladhadium and H. E. Jackson, Appl. Phys. Lett., 59: 1170 (1991).
142. P. Bou, L. Vandenbulcke, R. Herbin and F. Hillion, J. Mater. Res., 7: 2151 (1992).
143. R. C. Hyer, M. Green, K. K. Mishra and S. C. Sharma, J. Mater. Sci. Lett., 10: 515 (1991).
144. S. I. Shah and M. M. Waite, Appl. Phys. Lett., 61: 3113 (1992).
145. H. R. Thorsheim and J. E. Butler, Synthetic Diamond: Emerging CVD Science and Technology (K. E. Spear and J. P. Dismukes, ed.), John Wiley & Sons, Inc., New York, p. 193 (1994).
146. T. Kawato and K. Kondo, Jpn. J. Appl. Phys., 26: 1429 (1987).
147. S. J. Harris, D. N. Belton and A. M. Weiner, J. Appl. Phys., 66: 5353 (1989).
148. C. H. Wu, M. A. Tamor, T. J. Potter and E. W. Kaiser, J. Appl. Phys., 68: 4825 (1990).

149. L. Schafer, C.-P. Klages, U. Meier and K. Kohse-Hoinghaus, Appl. Phys. Lett., 58: 571 (1991).

150. K.-H. Chen, M.-C. Chuang, C. M. Penney and W. F. Banholzer, J. Appl. Phys., 71: 1485 (1992).

151. F. G. Celii and J. E. Butler, New Diamond Science and Technology (R. Messier, J. E. Butler and J. T. Glass, ed.), Materials Research Society, Pittsburgh, p. 201 (1991).

152. E. J. Corat and D. G. Goodwin, J. Appl. Phys., 74: 2021 (1993).

153. E. H. Wahl, T. G. Owano, C. H. Kruger, P. Zalicki, Y. Ma and R. N. Zare, Diam. Related Mater., 5: 373 (1996).

154. P. Zalicki and R. N. Zare, J. Chem. Phys., 102: 2708 (1995).

155. S. O. Hay, W. C. Roman and M. B. Colket III, J. Mater. Res., 5: 2387 (1990).

156. T. DebRoy, T. K., W. A. Yarbrough and R. Messier, J. Appl. Phys., 68: 2424 (1990).

157. U. E. Meier, L. E. Hunziker, D. R. Crosley and J. B. Jeffries, "Observation of OH Radicals in a Filament-Assisted Diamond Growth Environment," Proceedings of Second International Symposium on Diamond Materials, Washington, DC, p. 202 (1991).

158. K. Yarina, "Low Pressure Combustion CVD of Diamond," M.S. Thesis, Colorado State University (1996).

159. L. S. Plano, D. A. Stevenson and J. R. Carruthers, "Characterization of DC Plasmas for the Control of Diamond Deposition," Proceedings of Second International Symposium on Diamond Materials, Washington, DC, p. 290 (1991).

160. A. Inspektor, Y. Liou, T. McKenna and R. Messier, Surf. Coating Technol., 39/40: 211 (1989).

161. M. C. McMaster, W. L. Hsu, M. E. Coltrin, D. S. Dandy and C. Fox, Diam. Related Mater., 4: 1000 (1995).

162. K. R. Stalder and W. Homsi, Appl. Phys. Lett., 68: 3710 (1996).

163. J. A. Mucha, D. L. Flamm and D. E. Ibbotson, J. Appl. Phys., 65: 3448 (1989).

164. Y. Muranaka, H. Yamashita, K. sato and H. Miyadera, J. Appl. Phys., 67: 6247 (1990).

165. S. W. Reeve, W. A. Weimer and D. S. Dandy, J. Mater. Res., 11: 694 (1996).

166. W. Zhu, A. Inspektor, A. R. Badzian, T. McKenna and R. Messier, J. Appl. Phys., 68: 1489 (1990).

167. F. G. Celii, H. R. Thornsheim, J. E. Butler, L. S. Plano and J. M. Pinneo, J. Appl. Phys., 68: 3814 (1990).

168. H. R. Thorsheim, F. G. Celii, J. E. Butler, L. S. Plano and J. M. Pinneo, New Diamond Science and Technology (R. Roy, R. Messier, J. E. Butler and J. T. Glass, ed.), Materials Research Society, Pittsburgh, p. 207 (1991).

169. D. S. Green, T. G. Owano, S. Williams, D. G. Goodwin, R. N. Zare and C. H. Kruger, Science, 259: 1726 (1993).

170. T. Mitomo, T. Ohta, E. Kondoh, K. Ohtsuka and Y. Habu, J. Appl. Phys., 70: 4532 (1991).

171. K. R. Stalder and R. L. Sharpless, J. Appl. Phys., 68: 6187 (1990).

172. S. W. Reeve and W. A. Weimer, J. Vac. Sci. Technol. A, 12: 3131 (1994).

173. H. N. Chu, E. A. Den Hartog, A. R. Lefkow, J. Jacobs, L. W. Anderson, M. G. Lagally and J. E. Lawler, Phys. Rev. A, 44: 3796 (1991).

174. G. A. Raiche and J. B. Jeffries, Appl. Opt., 32: 4629 (1993).

175. G. P. Smith and J. B. Jeffries, Electrochem. Soc. Proc., 91-8: 194 (1991).

176. S. W. Reeve and W. A. Weimer, J. Vac. Sci. Technol. A, 13: 359 (1995).

177. R. S. Yalamanchi and K. S. Harshavardhan, J. Appl. Phys., 68: 5941 (1990).

178. Y. Hirose, S. Amanuma and K. Komaki, J. Appl. Phys., 68: 6401 (1990).

179. K. Komaki, Y. Masaaki, I. Yamamoto and Y. Hirose, Jpn. J. Appl. Phys., 32: 1814 (1993).

180. Y. Matsui, A. Yuuki, M. Sahara and Y. Hirose, Jpn. J. Appl. Phys., 28: 1718 (1989).

181. Y. Matsui, H. Yabe and Y. Hirose, Jpn. J. Appl. Phys., 29: 1552 (1990).

182. P. W. Morrison, J. E. Cosgrove, J. E. Markham and P. R. Solomon, New Diamond Science and Technology (R. Roy, R. Messier, J. E. Butler and J. T. Glass, ed.), Materials Research Society, Pittsburgh, p. 219 (1991).

183. N. G. Glumac and D. G. Goodwin, Materials Letters, 18: 119 (1993).

184. J. S. Kim and M. A. Cappelli, Appl. Phys. Lett., 65: 2786 (1994).

185. K. F. McCarty, E. Meeks, R. J. Kee and A. E. Lutz, Appl. Phys. Lett., 63: 1498 (1993).

186. D. G. Goodwin and G. G. Gavillet, J. Appl. Phys., 68: 6393 (1990).

187. W. L. Hsu, "Quantitative Analysis of the Gaseous Composition during Filament-Assisted Diamond Growth," Proceedings of Second International Symposium on Diamond Materials, Washington, DC, p. 217 (1991).

188. B. Ruf, F. Behrendt, O. Deutschmann and J. Warnatz, J. Appl. Phys., 79: 7256 (1996).

189. K. Tankala and T. DebRoy, J. Appl. Phys., 72: 712 (1992).

190. C. Wolden, S. Mitra and K. K. Gleason, J. Appl. Phys., 72: 3750 (1992).

191. Y. A. Mankelevich, A. T. Rakhimov and N. V. Suetin, "Two-Dimensional Model of a HFCVD Reactor," Proceedings of Fourth International Symposium on Diamond Materials, Reno, NV, p. 687 (1995).

192. T. Otsuka, M. Ihara and H. Komiyama, J. Appl. Phys., 77: 893 (1995).

193. D. G. Goodwin, Appl. Phys. Lett., 59: 277 (1991).

194. D. S. Dandy and M. E. Coltrin, Appl. Phys. Lett., 66: 391 (1995).

195. Y. A. Mankelevich, A. T. Rakhimov and N. V. Suetin, Diam. Related Mater., 4: 1065 (1995).

196. Y. A. Mankelevich, A. T. Rakhimov and N. V. Suetin, Plasma Phys. Rep., 21: 872 (1995).

197. S. L. Girshick, B. W. Yu, C. Li and H. H., Diam. Related Mater., 2: 1090 (1992).

198. B. W. Yu and S. L. Girshick, J. Appl. Phys., 75: 3914 (1994).

199. E. Meeks, R. J. Kee, D. S. Dandy and M. E. Coltrin, Combust. Flame, 92: 144 (1993).

200. M. Murayama, S. Kojima and K. Uchida, J. Appl. Phys., 69: 7924 (1991).

201. N. G. Glumac and D. G. Goodwin, Combust. Flame, 105: 321 (1996).

202. C. Wild, P. Koidl, W. Müller-Sebert, H. Walcher, R. Kohl, N. Herres, R. Locher, R. Samlenski and R. Brenn, Diam. Related Mater., 2: 158 (1993).

203. M. Yoshikawa, Diam. Films and Technol., 1: 1 (1991).